DELHI TECHNOLOGICAL UNIVERSITY

(formerly Delhi College of Engineering)

NEW DELHI

दिल्ली प्रौद्योगिकी विश्वविद्यालय, नई दिल्ली

Department of Applied Physics

THE ROLE OF DUST GRAINS ON THE EFFECT OF A LARGE AMPLITUDE LANGMUIR WAVE ON THE WEIBEL INSTABILITY

Dissertation Submitted in partial fulfilment of the requirements

for the degree of

MASTER OF TECHNOLOGY

in

NUCLEAR SCIENCE AND ENGINEERING (NSE)

Submitted by:

Gyan Prakash Singh,

Reg. No. – 2K13/NSE/05

Under the guidance of:

Prof. Suresh C. Sharma

Head, Department of Applied Physics,

Delhi Technological University,

(formerly Delhi College of Engineering)

New Delhi - 110042.

July-2015

CERTIFICATE

This is to certify that work which is being presented in the dissertation entitled **ROLE OF DUST GRAINS ON THE EFFECT OF A LARGE AMPLITUDE LANGMUIR WAVE ON THE WEIBEL INSTABILITY** is the authentic work of **GYAN PRAKASH SINGH** under my guidance and supervision in the partial fulfillment of requirement towards the degree of **Master of Technology in Nuclear Science & Engineering** run by the Department of Applied Physics in Delhi Technological University during the year 2013-2015.

As per the candidate declaration this work has not been submitted elsewhere for the award of any other degree.

Prof. SURESH C. SHARMA
Head, Department of Applied Physics
Delhi Technological University

Delhi-110042

<u>DECLARATION</u>

I, hereby, declare that the work being presented in this dissertation, entitled "**the role of dust grains on the effect of a large amplitude Langmuir wave on the Weibel instability**", is an authentic record of my own work carried out under the guidance of **Prof. Suresh C. Sharma**, Head, Department of Applied Physics, Delhi Technological University (Formerly Delhi College of Engineering), Delhi. The work contained in this dissertation has not been submitted in part or full, to any other university or institution for award of any degree or diploma.

This dissertation work is submitted to **Delhi Technological University** (Formerly Delhi College of Engineering) in partial fulfillment for the **Master of Technology (M. Tech)** in **Nuclear Science and Engineering** during the academic year 2014-2015.

DATE:

PLACE: New Delhi

_____

(Signature and Name of Student)

Gyan Prakash Singh

(2K13/NSE/05)

ACKNOWLEDGEMENT

I take this opportunity to express my sincere gratitude to all those who have been instrumental in the successful completion of this dissertation.

Prof. Suresh C. Sharma, Head, Department of Applied Physics, Delhi Technological University (Formerly Delhi College of Engineering), Delhi, my dissertation guide, who has guided me in the successful completion of this dissertation. It is worth mentioning that he always provided me with the necessary guidance and support.

I would also like to express my gratitude to Gaurav kumar, Dhaivat Udayan Mandavia, Mrityunjay Singh and Rahul with whom I have had many insightful discussions, which have cleared my understanding of various topics in plasma. My thanks also goes to all my classmates who have made the atmosphere in my classes lively and thought provoking to all the named and many unnamed, my sincere thanks. Surely it is almighty's grace to get things done fruitfully.

<div style="text-align: right">

GYAN PRAKASH SINGH

2K13/NSE/05

M.Tech (NSE)

</div>

ABSTRACT

I have developed a model on "the role of dust grains on the effect of a large amplitude Langmuir wave on the Weibel instabilities in plasma with an electron beam".

I have found that the growth rate of the mode increases with relative density of the dust grains and dust grain density. In addition, the growth rate also increases with decreasing dust grain size.

TABLE OF CONTENTS

LIST OF FIGURES

LIST OF TABLES

NOTATIONS

e	=	electron charge
m_e	=	mass of electrons
ϕ_g	=	electrostatic potential
ϕ_{Gp}, ϕ_{Gpb}	=	pondermotive potential
E	=	normalized electric field
ω_{G0}	=	angular frequency
ω_{Gpp}	=	angular phase frequency of pump wave
ω_{Gpb}	=	angular phase frequency of beam
ω_c	=	electron cyclotron frequency
ω_{Gp}	=	electron phase frequency
ω_{Gpi}	=	ion phase frequency
n_{Ge}	=	initial electron density distribution
n_{Gi}	=	initial ion density distribution
c	=	speed of light
ε_0	=	free space permittivity
ε_{G2}	=	upper sideband mode permittivity
χ_{Ge}	=	electron susceptibility
χ_{Gi}	=	ion susceptibility
χ_{Gb}	=	beam susceptibility
v_{Gte}	=	thermal velocity of electrons
F_{Gp}	=	pondermotive force
v_{Gti}	=	ion thermal velocity
λ_{GDi}	=	ion debye length
λ_{GDe}	=	electron debye length

n_{Gd} =   dust density

Q_{Gd} =   dust charge

ϕ_{Gp} =   ponderomotive potential

n_{Gb} =   beam electron density

v_{Gb} =   beam electron velocity

J_G^L =   linear current density

J_G^{NL} =   non-linear current density

v_G =   drift velocity

CHAPTER 1
INTRODUCTION

1.1 General

In plasma physics science, waves in plasmas are interconnected set of particles and fields which spreads and propagates in a periodically repeating fashion. A plasma is a quasi-neutral and electrically conductive fluid. In the most straightforward case, it is made out of electrons and a single species of positive ions, however it might contain multiple ion species including negative ions as well as neutral particles. A plasma couples to magnetic and electric field due to its electrical conductivity. A wide variety of wave phenomena is supported due to complex structure of particles and wave. Dusty plasma is a new frontier in modern technology and applied physics. The interaction between plasmas and charged dust grains has created a new and another captivating exploration area, that of a dusty or complex plasma.

Dusty plasma is one of the complex systems because of the variation of the mass, dust grain charge and shape and size with space and time. It shows new and unordinary behavior, and gives a possibility for modified or totally new collective modes of instabilities, oscillation and in addition coherent nonlinear structures. An interesting aspect of dusty plasma is that it can be emphatically coupled, that is the interaction potential energy between the dust grains can surpass their kinetic energy. As a result of which, grain–grain correlations become important; for sufficiently solid coupling, the dust grains can gather into a dusty plasma crystal configuration.

The dusty plasma can be billions of times heavier than that of the ions and acquire several thousands of electron charges. The dust grain charging take place due to a variety of physical processes including the collection of background plasma electrons and ions by dust grains, secondary electron emission, photoelectron emission, triboelectric charging, thermionic emission, and contact electrification, etc. In dust filled tornadoes and dust storms, dust particles e.g., sand get to be energized and become electrified as they rub each other when they are carried out by the air exchanging positive and negative charge. Thus, there is a possibility of charging dust grains as negatively or positively. The dust grains act as a origin of electrons when they are charged positively because of the irradiation of ultraviolet (UV) radiation or by thermionic emission. The charging of dust grain is a newly nonstationary physical process in dusty plasma.

Dusty plasmas are ubiquitous in different parts of our vast surroundings, for example, in the planetary ring system of Saturn, in the dust rings of the Martian moon Phobos, in Jupiter's moon, in circumsolar rings and interplanetary media, in cometary comet and tails, in supernova remnants, and in interstellar molecular clouds. Meteoritic dust is thought to be available in the Earth's mesosphere at heights of 80–95 km. It has been guessed that in the cold summer mesopause ice can be grown on meteoritic dust particles. The vicinity of charged dust particles in the polar summer mesopause has been conjured to clarify and explain the aspects of the very strong polar summer radar echoes alluded to as polar mesosphere summer echoes, which happen at elevations somewhere between 80 and 93 km. As of late, the presence of charged dust has been accounted in the mesosphere by direct rocket probe measurements consisting both negatively and positively charged dust grains.

Special modes of rocket engine operation infuse into the air and the atmosphere large amounts of burning items and combustion products at times in the order of hundreds of kilograms which can be in the form of solid particles or ice. Since the dust is shot out into the ionosphere with rapid and high speed relative to the background plasma in the order of km/s and the dust may be driven instabilities as it becomes charged. The development of artificial dusty plasma in the ionosphere was also uncovered and revealed during the Spacelab 2 mission when the space shuttle orbital maneuver system engines were fired, and the formation of large droplets and smaller and submicron fog was observed during a liquid water dump by the Discovery space shuttle. There are a number of future missions as the dust particles are a main element of interest in the interstellar medium and in the solar system. Dusty plasmas can also occur in the zodiacal light, in the flame of a humble candle, in cloud-to-ground lightning in thunderstorms, in volcanic eruptions, and in ball lightning. It has been proposed by that ball lightning is caused by oxidation of nanoparticle systems from ordinary lightning strikes on soil.

Dusty plasmas are experienced in mechanical and industrial applications as well, e.g., in such innovations as microelectronics including carbon nanotubes, as precipitation of vaporized particles in the combustion products of electric power stations, in electrostatic painting and in plasma spraying. Besides, there are additionally developing utilizations of charged dust in microbiology, in medicine, as well as in nanomedicine. In particular, an electro physical process, which includes the electrostatic tension on charged bodies the bacteria cells in dusty plasma, may be responsible for killing bacteria.

Dust grains with size distributions have additionally been seen in fusion plasmas. Charged dust grains, which may be made because of the sputtering of tokamak walls and which are made out of the berelium and carbon tiles can also behave as radioactive. It is, therefore, most likely that a small fraction of dust grains play a unique role in realizing the transport processes in high density and low-temperature tokamak edges. Charged dust grains present in tokamak edges are lifted from the base of the fusion machine and undergo acceleration, as a result of the sheath electrostatic and ion wind forces.

1.2 Historical Background

Tonks and Langmuir first coined the term 'plasma' around 70 years ago to describe the inner region of a glowing ionized gas produced by means of an electric discharge in a tube. The term "plasma" represents a macroscopically neutral gas containing numerous interacting charged particles and neutrals. It is likely that 99 percent of the matter in our universe is in the form of plasma. In this way, in most cases plasma exists together with the dust particulates. These particulates may be as big and large as a micron. They are not neutral but are charged either negatively or positively depending on their encompassing plasma situations. An admixture of such charged dust or macro-particles, ions, electrons and neutrals forms a 'dusty plasma'. A bright comet detected by our distant ancestors is an excellent cosmic laboratory for the analysis of dust–plasma interactions and their dynamical and physical consequences. Alternate indications of dust-laden plasmas analyzed by the ancients would have been the zodiacal light, the Orion Nebula , the noctilucent clouds, etc. A practically staggering number of images of astrophysical have recently been observed by the Hubble Space Telescope and spacecraft. Observations of dust-laden plasmas in the laboratory were additionally accessible in the remote past. The way that an ordinary flame is considered as plasma may come as a surprise because of the high-level of collision within it. However, the fact that makes it close to being a plasma is the presence of minute (~ 100 A$^\circ$) particles of unburnt carbon (soot). While the yellow light emitted by typical hydrocarbon flames because of incandescence of these small particulates heated over $1000^\circ C$. Thus, it is astonishing that the people of old considered fire as a fourth state of matter, while we have given this designation to plasma only about 70 years ago. There are a number of more recent examples of dust-laden plasmas in our surrounding. These are rocket and space shuttle exhausts, processing plasmas used in

device fabrications, thermonuclear fireballs, dusty plasmas created in laboratories for studying basic collective processes, plasma crystals, etc.

1.3 Formation of Plasma

Much the same as the many uses of plasma, there are several methods for its generation, however, one basic standard is common to all of them: there must be energy input to generate and sustain it. In this case, plasma is generated when an electric current is connected over a dielectric gasor fluid (an electrically non-conducting material) as can be seen in the figure, which shows a discharge tube as a simple example (DC used for simplicity).
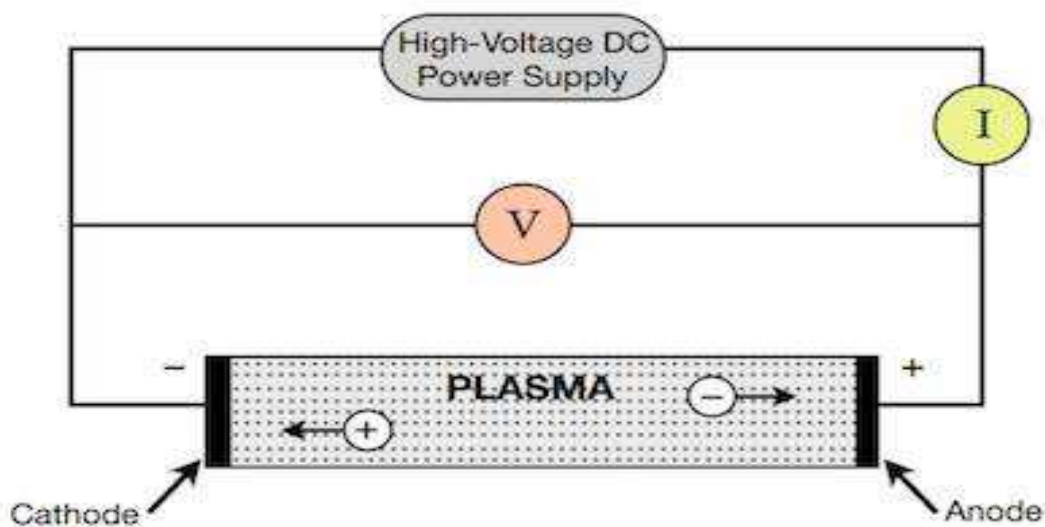
Figure 1.1 High voltage D.C. generation of plasma[32]

The potential difference and applied electric field attract the bound electrons (negative) toward the anode (positive electrode) while the cathode (negative electrode) attracts the nucleus. As the voltage increases further, the current stresses the material used (by electric polarization) beyond its dielectric limit (in term of strength) into a stage of electrical breakdown which leads to an electric spark where the material transforms from being an insulator into a conductor (as it becomes increasingly ionized). The underlying process is called as the Townsend avalanche in which collisions between

electrons and neutral gas atoms create more and more ions and electrons. The first collision of an electron on an atom results in one ion and two electrons. Therefore, the number of charged particles generated and increases rapidly (in the millions) only "after about 20 successive sets of collisions" is mainly due to a small mean free path (average distance travelled between collisions). With ample current density and ionization, there is formation of a luminous electric arc (a continuous electric discharge similar to lightning) between the electrodes. Heat is produced due to electrical resistance along the continuous electric arc which create more gas molecules and ionizes the resulting atoms (where degree of ionization is determined by temperature), and as per the sequence of formation: solid-liquid-gas-plasma, the gas is gradually turned into a thermal plasma. Thermal plasma is present in thermal equilibrium, which shows that the temperature is relatively homogeneous throughout the heavy particles (i.e. atoms, molecules and ions) and electrons. This happens because when thermal plasmas are generated, electrical energy is transferred to electrons which due to their great mobility and present in large numbers are able to disperse it rapidly and by elastic collision (without energy loss) to the heavy particles.

1.4 Formation of Dust Grain

Understanding the origination of dust grains in laboratory experiments as well as in our solar system is of fundamental interest. Planets form from dust and the nebula of gas that comprises the nascent solar system. Inelastic that is adhesive collisions between the dust particles form kilometer-sized planetesimals which then further collide under the influence of their mutual gravity to form planets. On the other hand, in low temperature laboratory plasma discharges dust particles can be developed utilizing reactive gases like ion bombardment on materials. It has been studied the growth of dust particles in laboratory discharges. For gas densities and temperatures that are typical of the nebula from which the solar system was formed. The dust particles appears like tiny cauliflowers squeezed together in irregular strings—a growth pattern that offers clues to the rate at which dust particles in interstellar space transformed into the clumps of matter that are large enough to assemble into planets because of gravity. Dust particles are charged because of a variety of processes including the bombardment of the dust grain surface by background plasma ions and electrons, photo electron emission by UV

radiation, secondary electron production, ion sputtering, etc. In low-temperature laboratory dust particles of dusty plasma usually acquire a negative charge because of the thermal speed of the electrons is much greater than that of the ions. The charging of dust grain depends on the charging cross section and is determined by the impact parameter of the ions and electrons that approach the dust grain to distances lesser than the dust particle size.

1.5 Characteristic of Dusty Plasma

A dusty plasma is approximately characterized as a normal electron–ion plasma with an extra charged component of micron- or submicron-sized particulates. This additional component of macro-particles increases the complexity of the system. This is the reason a dusty plasma is also referred to as a 'complex plasma'. Dusty plasmas are low temperature fully or partially ionized electrically conducting gases which are made up of electrons, ions, charged dust grains and neutral atoms. Dust grains are massive times and their shape and sizes range from nanometers to millimeters. Dust grains may be conducting, metallic or made of ice particulates. The shape and size of dust grains will be different and diverse, unless they are man-made. However in any case, when viewed from afar they can be considered as point charges.

A plasma with grains or dust particles can be termed as either 'a dusty plasma' or 'dust in a plasma' depending on the ordering of a number of characteristic lengths. These are the average inter-grain distance *(a)*, the dust grain radius (r_d), the plasma Debye radius (λ_D) and the dimension of the dusty plasma. The situation $r_d << \lambda_D < a$ corresponds to 'dust in a plasma', while the situation $r_d << a < \lambda_D$ corresponds to 'a dusty plasma'. While consider a plasma with isolated dust grains ($a >> \lambda D$), it should be taken into account the local plasma inhomogeneities. On the other side, while consider the opposite situation ($a << \lambda D$), it should be treated dust grains as massive charged particles similar to multiply charged negative or positive ions. The basic differences between an electron–ion (or multi-ion) plasma and a dusty plasma are pointed out in the form of table shown below. The table indicates that there subsists some distribution for the dust grain charge–mass ratio (q_d/m_d). The interaction among dust grains is checked by the background electrons and ions. The existence of charged dust grains does not only modify the presence low-frequency waves

Table 1: Difference between Electron-ion plasma and Dusty plasma[30]

Characteristics	Electron–ion plasma	Dusty plasma
Quasi-neutrality condition	$n_{e0} = Z_i n_{i0}$	$Z_d n_{d0} + n_{e0} = Z_i n_{i0}$
Massive particle charge	$q_i = Z_i e$	$|q_d| = Z_d e \gg q_i$
Charge dynamics	$q_i = $ constant	$\partial q_d / \partial t = $ net current
Massive particle mass	m_i	$m_d \gg m_i$
Plasma frequency	ω_{pi}	$\omega_{pd} \ll \omega_{pi}$
Debye radius	λ_{De}	$\lambda_{Di} \ll \lambda_{De}$
Particle size	uniform	dust size distribution
$E \times B_0$ particle drift	ion drift at low B_0	dust drift at high B_0
Linear waves	IAW, LHW, etc	DIAW, DAW, etc
Nonlinear effects	IA solitons/shocks	DA/DIA solitons/shocks
Interaction	repulsive only	attractive between grains
Crystallization	no crystallization	dust crystallization
Phase transition	no phase transition	phase transition

(e.g. lower hybrid waves (LHW), ion-acoustic waves (IAW), ion-acoustic (IA) solitons/shocks, etc.), but also introduces new types of low-frequency dust-related waves (e.g. dust IA waves (DIAW), dust acoustic waves (DAW), dust acoustic (DA) solitons/shocks, dust ion acoustic (DIA) solitons/shocks, etc) and associated instabilities. To analyze the characteristics of a dusty plasma properly, some basic characteristics have to re-examine, such as macroscopic neutrality, characteristic frequencies, Debye shielding, Coulomb coupling parameter, etc.

The components of dusty plasmas are neutral gas molecules, ions, electrons and massive when compared to the ions charged dust grains. There are three characteristic for such an admixture of dust and plasma. These are the dusty plasma Debye radius D, the dust grain radius R, and the average inter-grain distance d. The latter is related to the dust number density n_{d0} by $d=(3/4n_{d0})^{1/3}$. The Debye radius D in dusty plasma is given by

$$\frac{1}{\lambda_D^2} = \frac{1}{\lambda_{Di}^2} + \frac{1}{\lambda_{De}^2}$$

where $D_e = (T_e / 4\pi n_{e0} e^2)^{1/2}$ and $D_i = (T_i / 4\pi n_{i0} e^2)^{1/2}$ are the electron and ion Debye radius, respectively, Ti and Te are the ions and electron temperatures in the energy

unit, n_{i0} and n_{e0} are the unperturbed ion and electron number densities, and e is the magnitude of the electron charge. One can consider the dust from a particle dynamics point of view when $R \ll \lambda_d < d$, and in that case a plasma containing a dust in a plasma or isolated screened dust grains. On the other hand, it becomes important when $R \ll d < \lambda_d$ for collective effects of charged dust grains. Presently, charged dust grains which are considered to be essential ingredients of the total plasma mixture can be treated as a dust fluid identical to multiply charged negative or positive ions in multispecies plasma. The equilibrium quasi-neutrality condition in the presence of negatively charged dust grains is given by

$$Z_i n_{io} = n_{eo} + Z_{do} n_{do}$$

where Z_{d0} is the number of charges residing on the dust grain and Z_i is the ion charge state. When mostly electrons from the ambient plasma are attached to the dust grain, it has $Z_{d0}n_{d0} \gg n_{e0}$. The dusty plasma may be considered approximately as two-component plasma made up of negatively charged dust grains and positive ions. Such a situation may be common in planetary systems e.g. F ring of Saturn as well as in some low temperature dusty plasma discharges. On the other hand, the grains emit electrons in UV irradiated dusty plasmas and they can be charged positively.

CHAPTER 2

LITERATURE REVIEW

2.1 General

Recent experiments on the interaction of high power short pulse laser with under dense plasmas have revealed strong flows of relativistic electrons with energies up to a few tens of MeV and large thermal spread. The studies are relevant to fast ignitor concept of fusion, where an intense laser pulse passes through an under dense plasma and its relativistic self-channeling is accompanied by a high-energy (multi MeV) electron beam that propagates in the direction of the laser. This equilibrium, however, is liable to Weibel instability that may produce low scale length magnetic fields. The theory of Weibel instability under different conditions has been reported in literature. Ferrante *et al* have, recently, reported the theory of Weibel instability for a plasma interacting with an ultra-short laser pulse. Taguchi *et al* have reported the simulation results of a 2D code where a cylindrical solid hot electron beam propagating in a high density plasma evolves into a hollow, annular beam due to Weibel instability and generates strong magnetic field on both sides of annular ring. The ring subsequently breaks up into several beamlets. Sentoku *et al* have also reported the result of 2D PIC simulation of magnetic instability by the relativistic electron stream. They show that the kinetic effects of electrons on the magnetic instability to reduce the growth rate.

Annou and Tripathi [1], have explained The effect of a large amplitude Langmuir wave on the Weibel instability in a plasma with an electron beam is studied. The electromagnetic perturbation couples to the Langmuir wave to give rise to two Langmuir sideband waves, which in turn produce a current enhancing the electromagnetic perturbation. The Langmuir wave enhances the growth over its linear value. The enhancement is larger at shorter wavelengths. For $V_o/c \sim 0.15$, the growth rate is enhanced by a factor of 3/2.

Upadhyay and Tripathi[2], have presented the strong flows of relativistic electrons, encountered in high power short pulse laser plasma interaction, have the potential to drive Weibel instability producing short wavelength magnetic fields. The presence of a Langmuir wave couples the Weibel instability to two electrostatic wave sidebands. The density perturbations due to the sidebands couple with the oscillatory electron velocity due to the pump to produce a current that enhances the growth rate of Weibel instability. The thermal spread of the energetic (drifting) electrons, however, reduces the growth rate.

Sharma et al. [3], have studied the surface plasma wave excitation via Cerenkov and fast cyclotron interaction by a density modulated electron beam propagating through a magnetized dusty plasma cylinder. The dispersion relation of surface plasma waves has been derived and it has been shown that the phase velocity of waves increases with increase in relative density $\delta(= n_{io}/n_{e0}$, where n_{i0} is the ion plasma density and n_{e0} is the electron plasma density) of negatively charged dust grains. The beam radius is taken slightly less than the radius of dusty plasma cylinder. The frequency and the growth rate of the unstable wave instability increases with increase in the value of δ and normalized frequency ω/ω_{pe}. The growth rate of the instability increases with the beam density and scales as one-third power of the beam density in Cerenkov interaction and square root of beam density in fast cyclotron interaction. The dispersion relation of surface plasma waves has been retrieved from the derived dispersion relation by considering that the beam is absent and there are no dust grains in the plasma cylinder.

Tripathi and Liu [4], have discussed the resonance ($\omega o \approx \omega_p$) a high amplitude plasma wave decays into a purely growing electromagnetic perturbation and two Langmuir wave sidebands. The instability has a growth rate $\gamma = \omega_p K_o^2 |V_o|^2 / 8K^2 V_e^2$ for a Langmuir pump of finite wavenumber $ko > k\, v_e/c$, and for $\gamma = \omega_p |V_o|^2 / 16c^2$ a laser light pump. In the latter case, the instability has an inhomogeneity threshold $|V_o|^2 \omega_p L / 2c^3 = 1$ and is a source of spontaneous generation of magnetic field.

Leemans et al.[5], have analysed the tunneling-ionization model predicts that fully ionized plasmas with controllable perpendicular ($T_\perp$) and negligible longitudinal temperature ($T_\parallel$) can be produced. The validity of these predictions has been studied through experiments and supporting theory and simulations. Emission of odd harmonics of the laser frequency, indicative of a stepwise ionization process, has been observed. X-ray measurements show that the plasma temperature is higher for a circularly polarized laser-produced plasma compared to when linear polarization is used. Analytically we find that the growth of the stimulated Raman (SRS) and Compton scattering (SCS) instabilities are suppressed during the ionization phase. A higher $T_\parallel$ than expected from the single-particle-tunneling model was observed after the ionization phase through SCS fluctuation

spectra. The maximum achievable plasma density is found to be limited by ionization induced refraction. One-dimensional (1D) simulations show that, after the ionization phase, the initial $T_\parallel$ is low as expected from the single particle model and SRS density fluctuations grow to large values. In 2D simulations, however, $T_\parallel$ at the end of the ionization phase is already much higher and only SCS is seen to grow. The simulations indicate that stochastic heating and the Weibel instability play an important role in plasma heating in all directions and in making the plasma isotropic. Two-dimensional simulations also confirm that refraction plays a crucial role in determining the maximum electron density that can be obtained in such plasmas.

Sharma et al. [6], have presented a density-modulated electron beam propagating through a plasma cylinder excites surface plasma waves SPWs via Cerenkov and fast cyclotron interaction. A nonlocal theory of this process has been developed. Numerical calculations of the growth rate and unstable mode frequencies have been carried out for the typical parameters of the SPWs. The growth rate γ (in rad/s) of the unstable wave instability increases with the modulation index Δ and has the largest value for $\Delta=1$ in addition to when the frequency and wave number of the modulation are comparable to that of the unstable wave. For $\Delta=0$, γ turns out to be $\sim 6.06\times10^9$ rad/s for Cerenkov interaction and $\sim 5.47\times10^9$ rad/s for fast cyclotron interaction. The growth rate of the instability increases with the beam density and scales as one-third power of the beam density in Cerenkov interaction and is proportional to the square root of beam density in fast cyclotron interaction. The real part of the frequency of the unstable wave increases as almost the square root of the beam voltage. The results of the theory are applied to explain some of the experimental observations.

Sharma and Walia [7], have studied a spiraling ion beam propagating through a magnetized dusty plasma cylinder drives electrostatic lower hybrid waves to instability via cyclotron interaction. Numerical calculations of the growth rate and unstable mode frequencies have been carried out for the Princeton Q-1 device using theexperimental dusty plasma parameters. It is found that as the density ratio $\delta=n_{io}/n_{eo}$, where n_{i0} is the ion plasma density and n_{e0} is the electron density of negatively charged dust grains to electrons increases, the unstable mode frequency of the lower hybrid waves increases. In addition, the growth rate of the instability also increases with the density ratio. In other words, the presence of negatively charged dust grains can further destabilize the lower

hybrid wave instability. The growth rate has the largest value for the modes where $J_l(p_n r_o)$ is maximum [here $p_n = x_n/r_0$, where p_n is the perpendicular wave number in cm^{-1}, r_0 is the plasma radius, and x_n are the zeros of the Bessel function $J_1(x)$]i.e., whose eigenfunctions peak at the location of the beam. The growth rate scales as one third power of the beam current.

Sharma and Sugawa [8], have analysed an ion beam propagating through a magnetized dusty plasma cylinder drives electrostatic dust ioncyclotron waves to instability via Cerenkov interaction. The growth rate of the instability increases with the relative density δ ($= n_{0i}/n_{0e}$) of negatively charged dust. The growth rate scales as the one-third power of the beam density. The frequency of the unstable wave also increases with the relative density d of negatively charged dust.

Liu and Tripathi [9], have discribed laser incident on a metal film (deposited on a glass substrate) from the glass side at a specific angle of incidence, excites a surface plasma wave (SPW) at the metal-free space interface. The ratio of the SPW field to the laser field increases with the laser spot size attaining a value much greater than one at b>exp(2ωa/c) where is the film thickness and is the laser frequency. The SPW (ω, K_z) can also be excited by a relativistic electron beam, propagating parallel to the interface in the free space region, via Cerenkov interaction when beam energy $\in_b = (\in -1)mc^2$ where is the effective metal permittivity, and mc^2 is the electron rest mass energy. When the surface has a ripple of wave number K_0, the SPW can be excited at lower beam energy via sideband coupling, $\omega = (K_z + K_o) v_b$ where $v_b \hat{z}$ is the beam velocity. In both cases, however, the positioning of the beam in the close proximity of the interface is required. The scheme is useful for the generation of wavelengths longer than 1 m.

Sharma and Srivastava [10], have studied an ion beam propagating through a magnetized plasma cylinder containing K$^+$ positive ions, electrons and SF$_6$negative ions drives electrostatic ion-cyclotron (EIC) waves to instability via Cerenkov interaction. Two EIC wave modes are present, the SF$_6^-$ and K$^+$ modes. The frequencies and the growth rate of both the unstable negative ion and the positive ion modes increase, with increasing $\varepsilon(= n_{SF_6^-}/n_{K^+})$, the relative density of negative ions. The frequencies of both the unstable modes (SF$_6^-$ and K$^+$) increase, with the magnetic field. The growth rate of both the unstable modes (SF$_6^-$ and K$^+$) scales as the one-third power of the beam density. The real

frequency of both the unstable modes increases as almost the square root of the beam energy.

Prakash and Sharma [11], have analyzed an electron beam drives surface plasma waves to instability on a vacuum magnetized dusty plasma interface and in a magnetized dusty plasma cylinder via Cerenkov and fast cyclotron interaction. The dispersion relation of a surface plasma wave has been derived and it has been shown that the phase velocity of waves increases with increase in relative density $\delta = n_{i0}/n_{e0}$, where n_{i0} is the ion plasma density and n_{e0} is the electron plasma density of negatively charged dust grains. The frequency and the growth rate of the unstable wave instability also increases with δ. The growth rate of the instability increases with beam density and scales as the one-third power of the beam density in Cerenkov interaction and is proportional to the square root of beam density in fast cyclotron interaction. The dispersion relation of surface plasma waves has been retrieved from the derived dispersion relation by considering that the beam is absent and there is no dust in the plasma cylinder.

Tripathi et al. [12], have studied an intense short laser pulse incident on a metallic target produces an over dense plasma and excites a plasma surface wave via stimulated Compton scattering. The pump and the surface wave exert a beat-frequency ponderomotive force on the electrons in the skin layer, driving a heavily damped quasimode. The density perturbations due to the quasimode couple with the oscillatory velocity due to the pump to drive the surface wave. The growth period for the process turns out to be about 0.5 ps at a Nd:glass laser intensity of 10^{16} W cm^{-2} and a plasma density of 1.5 times the critical value.

Sharma et al. [13], have analyzed an electron beam propagating through a magnetized dusty plasma drives electrostatic lower hybrid waves to instability via Cerenkov interaction. A dispersion relation and the growth rate of the instability for this process have been derived taking into account the dust charge fluctuations. The frequency and the growth rate of the unstable wave increase with the relative density of negatively charged dust grains. Moreover, the growth rate of the instability increases with beam density and scales as the one-third power of the beam density.

Sharma and Sharma [14], have presented a spiraling ion beam propagating through a magnetized dusty plasma cylinder drives electrostatic ion cyclotron waves to instability via cyclotron interaction. Numerical calculations of the growth rate and unstable mode

frequencies have been carried out for the typical parameters of dusty plasma experiments in the two limits, namely, long parallel wavelength and short parallel wavelength. It is found that as the density ratio of negatively charged dust grains to electrons increases, the unstable mode frequency and the growth rate of the instability of the ion cyclotron waves increase in both the limits. The growth rate of the instability increases by a factor of 2.5 when the density ratio of negatively charged dust grains changes from 1.0 to 4.0 in the limit of short parallel wavelengths. Moreover, the growth rate increases with the density ratio of negatively charged dust at higher values in the present case in the limit of long parallel wavelengths. The growth rate of the unstable mode has the largest value for the modes whose eigen functions peak at the location of the beam. The growth rate of the instability scales as the one-third power of the beam current in both limits.

Anderson et al. [15], have summarizes experimental results on the injection and transport of intense, wide cross-section H^+ plasma (PB), and ion beams (IB), in vacuum and ambient H^+ plasma across an applied B-field. The injection of plasma and ion beams into magnetic confinement devices have the potential to heat and support current in these systems (e.g., field-reversed configurations). The translational energies of the PB and IB ranged between E_{pb}= 60 to 120 eV and E_{IB}= 60 to 120 keV, with temperatures and densities in the range of T_b 2~ to 10 eV, n_b ~10^{12} to 10^{13} cm^3, and T_b ~200 eV, n_b~ 10^{10} to 10^{11} cm^3, respectively. Compared to earlier, this research extends the experimental parameter space to higher beam current densities (up to 30 A/cm^2) and higher B-field strengths up to 1.6 kG. The PB and IB were both about 10 cm in diameter at the injection port, and the ratio of beam specific energy to ambient B-field specific energy, b, was in the range of 0.1 to 10. Ratios of beam Larmor radius to beam size, r, ranged from 10^{-1} to 1 and 1 to 10 for the PB and IB, respectively. Cross B-field propagation of the PB in vacuum was undeflected as a whole with a sharp increase (one order or more) in the current density of the central beam core at B-field levels > 1 kG accompanied by a significant loss of beam peripheral layers, beam "braking" and preferential beam expansion along the B-field lines. Cross B-field propagation of the PB in ambient plasma did not differ substantially from the case without B-field, that is, no deflection of the PB as a whole, which could be due to an insufficient neutralization of the induced E-field inside the PB. Cross B-field propagation of the IB in ambient plasma followed a single particle trajectory deflection with a simultaneous significant loss of IB intensity without any detectable bunching, indicating an adequate shorting of the polarization E-field inside the IB.

Anisimov et al. [16], have showed the excitation of surface waves by a moving laser beam has been studied both theoretically and experimentally. Using periodic surface structures (PSS) as an example. it is demonstrated that the type of excited wave and the rate of its growth depend resonantly on the beam velocity. Experimental data show that resonant excitation of different PSS can change the spatial distribution of the absorbed laser energy.

Bigongiari et al. [17], have explained the possibility of inducing a magnetic field via surface plasma-wave excitation is investigated with a simple nonrelativistic hydrodynamic model. A static magnetic field is predicted at the plasma surface, scaling with the square of the surface-wave field amplitude, and the influence of the electron plasma density is studied. In the case of resonant surface-wave excitation by laser this result can be applied to low intensities such that the electron quiver velocity in the field of the surface wave is less than its thermal velocity.

Bouhelier [18], have expressed that interfering surface Plasmon polaritons can be excited with a focused laser beam at normal incidence to a plane metal film. No protrusions or holes are needed in this excitation scheme. Depending on the axial position of the focus, the intensity distribution on the metal surface is either dominated by interferences between counter propagating Plasmon or by a two-lobe pattern characteristic of localized surface Plasmon excitation. Our experiments can be accurately explained by use of the angular spectrum representation and provide a simple means for locally exciting standing surface plasmon polaritons.

Boyd et al. [19], have analyzed the results of a theoretical and experimental investigation of the high-frequency interaction of an electron beam with a plasma are reported. An electron beam, modulated at a microwave frequency, passes through a uniform region of a mercury arc discharge after which it is demodulated. Exponentially growing wave amplification along the electron beam was experimentally observed.

Chen et al. [20], have studied that titanium nitride appears golden and has a high conductivity, the possibility that it can be used in surface plasma wave applications in a manner similar to gold but with very strong scratch-resistance, is of interest. This work considers this possibility using the Kretschmann configuration, measuring the angle-dependent reflectivity as well as the wavelength-dependent reflectivity. Both sets of

results demonstrate the excitation of a surface plasma wave at the TiN/air interface by an incident p-wave. The thickness of TiN that most efficiently couples the incident p-wave to the surface plasma wave is around 35 nm. All of the experiments are accompanied by corresponding numerical simulations.

Ezaki et al. [21], have studied the surface modification of semi-conductors by laser induced surface electromagnetic wave (SEW) etching was investigated. With the novel etching method using a holographic exposure system, submicron periodic dot structures were fabricated directly on semiconductor substrates (n-InP, n-GaAs, and InGaAs-InP). Making use of laser polarization dependence in this etching system, a variety of surface modifications could be achieved on the semiconductors. In particular, in the case of using the s-polarization light, periodic submicron dot structures with a geometrical diameter down to 80 nm could be obtained directly using a single-step process without a mask. The 1nGaA.s-InP dot structures were studied optically by means of photoluminescence spectroscopy, and the blue shift of the photoluminescence energy up to 5.36 meV was observed for the smallest dots, which displayed a lateral quantization.

Ghorbanalilu [22], have studied the goal of this theory is to study the conversion of a fraction of a laser beam to its phase-mismatch second and third harmonics. This conversion takes place by focusing an intense laser beam into a transversely magnetized plasma, as a nonlinear medium. The influence of the polarization field is considered, however, the plasma density is below the critical density. It has already been revealed that for dense plasma, the second and third harmonics efficiencies decreased with density increasing in the presence of a sufficiently strong magnetic field. This result is in contrast to the under dense and weakly magnetized plasma, which the harmonics efficiencies increased with density increasing. It is shown that the harmonics radiation cut-off, when the magnetic field increases up until the saturation strength Bsat. In addition, the results indicated that the average phase-mismatch third harmonic conversion efficiency is a little smaller than the phase-match case reported for non-magnetized plasma.

Girka et al. [23], have explained the excitation of ion azimuthal surface oscillations with extraordinary polarization by light ion beam is studied analytically. Beam-plasma system consists of a cylindrical metal waveguide filled partially by cold magnetized plasma and light ion flow rotating around the plasma column. Dependencies of the beam instability growth rateon the system parameters (plasma and beam densities, value of the external

axial magnetic field, radius of the plasma column, width of the gap between the plasma column and the waveguide wall, absolute value and sign of the azimuthal wave number) are analyzed numerically.

Girka et al. [24], have showed the excitation of extraordinarily polarized azimuthal surface eigenwaves is shown to be possible in the frequency range above the upper hybrid resonance in waveguides with metal walls which are partially filled by cold magnetoactive plasma. Interaction of these waves with flows of electrons which rotate around the plasma column in the narrow gap separating the plasma from the wall of the waveguide is studied. Conditions of resonant interaction of the beam with the mentioned high frequency azimuthal surface waves are shown by numerical methods to be reachable ones in the case of enough strong external magnetic fields without passing to the field of ultra-relativistic velocities of the beam.

Irvine and Elezzabi [25], have worked on the ponderomotive acceleration of electrons using surface plasmon sSPd waves launched on Ag and Au films. High-energy electrons, up to 2 keV, are generated in the high spatial gradient of the SP field. Acceleration gradients of ,8 GeV/m are produced using 30 GW/cm2, 800 nm amplified 30 fs laser pulses. Investigation of the photoemission characteristics of these metal films reveals a distinct transition between the multiphoton regime and a laser-induced field emission regime. Results of the experiment are in good agreement with those predicted with test particle code, which is based on finite-difference time-domain simulation and incorporates the Drude dielectric function and photoemission properties of the metallic films.

Jana et al. [26], have proposed highly charged dust grains immersed in a plasma can exhibit charge fluctuations in response to oscillations in the plasma currents flowing into them. This introduces a new physical effect, namely, the electric charge on the dust particles becomes time dependent and a self-consistent dynamical variable. The consequent modifications in the collective properties of a dusty plasma are investigated. It is shown that these effects lead to dissipative and instability mechanisms for ion waves in the plasma and can lead to interesting applications to many laboratory and astrophysical situations.

Krafft et al. [27], have worked on emission of whistler waves by a density modulated electron beam is studied in a laboratory plasma and compared to excitation by loop antenna. Single and double pole excitation are predicted by a simple linear model which

agrees with the experiments. The fraction of the power of the modulated beam radiated by the whistler wave has been measured and is of the order of 10^{-5}

Lee et al. [28], have described the effects of magnetic field strength on low-frequency surface ion plasma wave are investigated in semi-bounded magnetized dusty plasmas. The dispersion relation of the surface ion plasma wave is obtained by the plasma dielectric function with the specular reflection boundary condition. The results show that a transition from linear increase into the final level, i.e., the occurrence of a wave resonance. At a given frequency the phase velocity stays almost constant as long as the frequency remains below the respective resonance frequency.

Ostrikov et al.[29], have explained the effect of charged particulates or dusts on surface wave produced microwave discharges is studied. The frequencies of the standing electromagnetic eigenmodes of large-area flat plasmas are calculated. The dusts absorb a significant amount of the plasma electrons and can lead to a modification of the electromagnetic field structure in the discharge by shifting the originally excited operating mode out of resonance. For certain given proportions of dusts, mode conversion is found to be possible. The power loss in the discharge is also increased because of dust-specific dissipations, leading to a decrease of the operating mode quality factor.

Shukla et al. [30], have worked on Dusty plasmas are ubiquitous in low-temperature laboratory discharges as well as in the near-earth environment, planetary rings, and interstellar spaces. In this paper, updated knowledge of fundamentals of collective dust-plasma interactions and several novel phenomena are presented that have been observed in laboratories and in space dusty plasmas. Mechanisms that are responsible for the charging of dust grains are discussed, and the fact that the dust charge perturbation is a new dynamical variable in a dusty plasma. The underlying physics of different forces that act on a charged dust grain is reviewed. In dusty plasmas, there are new attractive forces e.g., due to wake field and ion focusing effects and dipole-dipole interactions between unevenly charged dust rods. Furthermore, in the presence of an ensemble of charged dust grains, there are collective dust-plasma interactions featuring new waves e.g., the dust acoustic wave, the dust ion-acoustic wave, the dust lattice wave, etc., new instabilities, and coherent nonlinear structures dust acoustic and dust ion-acoustic shocks, dust voids, and dust vortices, which are also discussed. Theoretical models for numerous collective dust-

plasma interactions are compared with existing observations from laboratories and space environments.

Smolyaninov [31], have described a new far-field optical microscopy technique capable of reaching nanometer-scale resolution has been developed recently using the in-plane image magnification bysurface plasmon polaritons. This microscopy is based on the optical properties of ametal-dielectric interface that may, in principle, provide extremely large values of the effective refractive index n_{eff} up to 10^2-10^3 as seen by the surface plasmons. Thus, the theoretical diffraction limit on resolution becomes λ $/2n_{eff}$, and falls into the nanometer-scale range. The experimental realization of the microscope has demonstrated the optical resolution better than 50 nm for 502 nm illumination wavelength. However, the theory of such surface plasmon-based far-field microscope presented so far gives an oversimplified picture of its operation. For example, the imaginary part of the metal's dielectric constant severely limits the surface-plasmon propagation and the shortest attainable wavelength in most cases, which in turn limits the microscope magnification. Here I describe how this limitation has been overcome in the experiment, and analyze the practical limits on the surface plasmon microscope resolution. In addition, I present more experimental results, which strongly support the conclusion of extremely high spatial resolution of the surface plasmon microscope.

2.2 Conclusion

This literature review provides a basic knowledge in the area of the role of dust grains on the effect of a large amplitude Langmuir wave on the Weibel instabilities in plasma with an electron beam. It provides a knowledge about types of control algorithms already implemented in past, there advantages, disadvantages, etc. This review provides knowledge about what are those parameters which can be controlled to provide better performance of the system.

Chapter 3

Role of Dust Grains on the Growth rate of the Instability

3.1 Introduction

In this dissertation, we have studied the role of dust grains on the effect of a large amplitude Langmuir wave of frequency $\omega_G \approx \omega_{Gp}$ on the Weibel instabilities in plasma with an electron beam. The Langmuir wave may be generated because of a parametric process such as Raman scattering or can be generated by a laser wave through linear mode conversion.

The electromagnetic perturbation pairs to the pump wave to produce two sideband waves which in turn generate a nonlinear current supporting the electromagnetic perturbation.

3.2 Analysis and dust charge calculation

In the present case, dust is consider unmagnetized because $\omega \sim \omega_{ci} >> \omega_{cD}$ with $\omega_{GcD} = \dfrac{Q_{Gd}B_0}{m_{0D}}$

where ω_{GcD} is dust gyro-frequency.

Now we applying probe theory for dust grain, the charge of dust grain Q_{Gd} is known to be balanced with the plasma currents on the dust grain surface as [26]

$$-\frac{Q_{Gd}}{dt} = I_{1e} + I_{1i}$$

The dust charge fluctuation is governed by the equation-

$$\frac{Q_{Gd}}{dt} + \eta_G Q_{Gd} = -\left|I_{Ge0}\right|\left(\frac{n_{Gi1}}{n_{Gio}} - \frac{n_{Ge1}}{n_{Geo}}\right)$$

where

$$\eta_G = \frac{\left|I_{Geo}\right|e}{C_g}\left[\frac{1}{T_e} + \frac{1}{T_i - e\phi_{go}}\right]$$

$Q_{Gd1} = Q_{Gd} - Q_{Gdo}$ is the perturbed dust grain charge,

$C_g = a\left(1 + \dfrac{a}{\lambda_{GeD}}\right)$ is the capacitance of the dust grain, a is the dust grain size and λ_{GeD} is the electron Debye length.

Substituting $d/dt = -i\omega$, we obtain the dust charge fluctuation Q_{Gd1}

considering the electron density, we obtain

$$Q_{Gd} = -\frac{|I_{Geo}|}{i(\omega + i\eta_G)}\left(-\frac{n_{Ge1}}{n_{Ge0}}\right)$$

following Annou and Tripathi [1], the perturbed electron density is given by

$$n_{Ge1} = \frac{k_1^2}{4\pi e}\left(-\frac{\omega_{Gpp}^2}{\omega_{G1}^2} - \frac{k_1^2 v_{Gth}^2}{\omega_{G1}^2}\right)$$

where

$$\omega_{Gpp} = \left(4\pi n^o{}_{Ge}e^2/m\right)^{1/2}$$

The wave equation is given as

$$-\nabla^2\vec{E} + (\nabla\cdot\vec{E})\vec{E} = \frac{4\pi i\omega}{c^2}(\vec{J}_G{}^L + \vec{J}_G{}^{NL}) + \frac{\omega^2}{c^2}\vec{E} \qquad (1)$$

following Annou and Tripathi [1], the value of linear and non-linear current density is given as

$$\vec{J}_G{}^{NL} = -\frac{1}{2}n_{G1}e\vec{v}_{G0} - \frac{1}{2}n_{G2}e\vec{v}_{G0} - \frac{1}{2}n_{G1b}e\vec{v}_{G0b} - \frac{1}{2}n_{G2b}e\vec{v}_{G0b}^*$$

$$= -\frac{k_1^2}{8\pi}\left(\chi_{G1}\phi_{g1}\vec{v}_{G0} + \chi_{G1b}\phi_{g1}\vec{v}_{G0b}\right) - \frac{k_2^2}{8\pi}\left(\chi_{G2}\phi_{g2}\vec{v}_{G0}^* + \chi_{G2b}\phi_{g2}\vec{v}_{G0b}\right)$$

and

$$\vec{J}_G{}^L = \frac{-e^2 E}{mi\omega}\left(n_G^0 + n_{Gb}^0 + n_{Gb}^0\frac{k^2 v_G^2}{\omega^2}\right)\hat{z} - n_{Gb}^0\frac{e^2}{mi\omega}\left(\frac{kv_G}{\omega}\right)E\hat{x}$$

where plasma electron susceptibility is $\chi_{G1} = \dfrac{-\left(\omega_{Gpp}^2 + k_1^2 v_{Gth}^2\right)}{\omega_{G1}^2}$

substituting the value of $\nabla \cdot \vec{E} = -4\pi n_{Gd} Q_{Gd}$, J_G^L and J_G^{NL} in Eq. (1), we obtain

$$k^2 \vec{E}_1 + \left(-4\pi n_{Gd} Q_{Gd}\right)\vec{E} = \frac{-4\pi i \omega}{c^2}\left\{\frac{e^2 E_1}{mi\omega}\left(n_G^0 + n_{Gb}^0 + n_{Gb}^0 \frac{k^2 v_G^2}{\omega^2}\right)\hat{z} + n_{Gb}^0 \frac{e^2}{mi\omega}\left(\frac{kv_G}{\omega}\right)E_1\hat{x}\right.$$

$$\left. + \frac{k_1^2}{8\pi}\left(\chi_{G1}\phi_{g1}\vec{v}_{G0} + \chi_{G1b}\phi_{g1}\vec{v}_{G0b}\right) + \frac{k_2^2}{8\pi}\left(\chi_{G2}\phi_{g2}\vec{v}_{G0}^* + \chi_{G2b}\phi_{g2}\vec{v}_{Gob}^*\right)\right\} + \frac{\omega^2}{c^2}\vec{E}_1$$

The linear response of the beam electrons for velocity and density[1]

$$v_{G1b} = -\frac{ek_1\phi_{g1}}{m(\omega G_1 - k_{1z}v_G)}$$

and $n_{G1b} = -\dfrac{n_{Gb}^o e k_1^2 \phi_{g1}}{m(\omega_{G1} - k_{1z}v_G)^2}$

$$k^2 \vec{E}_1 - \frac{\omega^2}{c^2}\vec{E}_1 + \frac{4\pi e^2 \vec{E}_1}{mc^2}\left(\frac{m\omega_{Gpp}^2}{4\pi e^2}\right) + \frac{4\pi e^2 \vec{E}_1}{mc^2}\left(\frac{m\omega_{Gpb}^2}{4\pi e^2} + \frac{m\omega_{Gpb}^2}{4\pi e^2}\frac{k^2 v_G^2}{\omega^2}\right)$$

$$= \frac{-4\pi i \omega}{c^2}\left\{\frac{k_1^2}{8\pi}\left(\chi_{G1}\phi_{g1}\vec{v}_{G0} + \chi_{G1b}\phi_{g1}\vec{v}_{G0b}\right) + \frac{k_2^2}{8\pi}\left(\chi_{G2}\phi_{g2}\vec{v}_{G0}^* + \chi_{G2b}\phi_{g2}\vec{v}_{Gob}^*\right)\right\} - \left(-4\pi n_{Gd}Q_{Gd}\right)\vec{E}$$

where $\omega_{Gpb} = \left(4\pi n^o{}_{Geb}e^2/m_e\right)^{1/2}$

$$k^2 - \frac{\omega^2}{c^2} + \frac{\omega_{Gpp}^2}{c^2} + \frac{\omega_{Gpb}^2}{c^2}\left(1 + \frac{k^2 v_G^2}{\omega^2}\right) = \frac{-4\pi i \omega}{c^2}\left\{\frac{k_1^2}{8\pi}\left(\chi_{G1}\phi_{g1}\vec{v}_{G0} + \chi_{G1b}\phi_{g1}\vec{v}_{G0b}\right) + \frac{k_2^2}{8\pi}\left(\chi_{G2}\phi_{g2}\vec{v}_{G0}^* + \chi_{G2b}\phi_{g2}\vec{v}_{Gob}^*\right)\right\}$$

$$+ \left(4\pi n_{Gd}\frac{|I_{Geo}|}{i(\omega + i\eta_G)}\left(-\frac{1}{n_{Geo}}\frac{k_1^2}{4\pi e}\chi_{G1}\phi_{g1}\right)\right)\vec{E} \tag{2}$$

where

$$\beta_G = \frac{|I_{Geo}|}{e} \frac{n_{Gdo}}{n_{Geo}} \qquad \text{is the coupling parameter}$$

The coupling parameter can be rewritten after using the charge neutrality condition and the value of equilibrium electron current as

$$\beta_G = 0.397(1 - \frac{1}{\delta_G}) \left(\frac{a}{v_{Gte}} \right) \omega_{Gpi}^2 \left(\frac{m_i}{m_e} \right)$$

$$k^2 - \frac{\omega^2}{c^2} + \frac{\omega_{Gpp}^2}{c^2} + \frac{\omega_{Gpb}^2}{c^2} \left(1 + \frac{k^2 v_G^2}{\omega^2} \right) = \frac{-4\pi i \omega}{c^2} \left\{ \frac{k_1^2}{8\pi} \left(\chi_{G1} \phi_{g1} \vec{v}_{G0} + \chi_{G1b} \phi_{g1} \vec{v}_{G0b} \right) + \frac{k_2^2}{8\pi} \left(\chi_{G2} \phi_{g2} \vec{v}_{G0}^* + \chi_{G2b} \phi_{g2} \vec{v}_{Gob}^* \right) \right\}$$
$$+ \left(\frac{\beta_G}{i(\omega + i\eta_G)} \left(-\frac{k_1^2}{1} \chi_{G1} \phi_{g1} \right) \right) \vec{E} \qquad\qquad (3)$$

Substituting the value of ϕ_{g1} and ϕ_{g2} [1], we get

$$k^2 - \frac{\omega^2}{c^2} + \frac{\omega_{Gpp}^2}{c^2} + \frac{\omega_{Gpb}^2}{c^2} \left(1 + \frac{k^2 v_G^2}{\omega^2} \right) = \frac{-4\pi i \omega}{c^2} \left\{ \frac{k_1^2}{8\pi} \phi_{g1} \left(\chi_{G1} \vec{v}_{G0} + \chi_{G1b} \vec{v}_{G0b} \right) + \frac{k_2^2}{8\pi} \phi_{g2} \left(\chi_{G2} \vec{v}_{G0}^* + \chi_{G2b} \vec{v}_{Gob}^* \right) \right\}$$
$$+ \left(\frac{\beta_G}{i(\omega + i\eta_G)} \left(\chi_{G1} \frac{k_1^2}{\varepsilon_{G1}} \left(\chi_{G1} \phi_{Gp_1} + \chi_{Gb_1} \phi_{Gp_{b1}} \right) \frac{k^2}{k_1^2} \right) \right) \vec{E}$$

$$k^2 - \frac{\omega^2}{c^2} + \frac{\omega_{Gpp}^2}{c^2} + \frac{\omega_{Gpb}^2}{c^2} \left(1 + \frac{k^2 v_G^2}{\omega^2} \right) = \frac{-4\pi i \omega}{c^2} \left\{ \frac{k_1^2}{8\pi} \phi_{g1} \left(\chi_{G1} \vec{v}_{G0} + \chi_{G1b} \vec{v}_{G0b} \right) + \frac{k_2^2}{8\pi} \phi_{g2} \left(\chi_{G2} \vec{v}_{G0}^* + \chi_{G2b} \vec{v}_{Gob}^* \right) \right\}$$
$$+ k^2 D_G^2$$

where

$$D_G^2 = \frac{\beta_G}{i(\omega + i\eta_G)\varepsilon_{G1}} \chi_{G1} \left(\chi_{G1} \phi_{Gp_1} + \chi_{Gb_1} \phi_{Gp_{b1}} \right) \vec{E} \qquad\qquad (4)$$

$$k^2 - \frac{\omega^2}{c^2} + \frac{\omega_{Gpp}^2}{c^2} + \frac{\omega_{Gpb}^2}{c^2}\left(1 + \frac{k^2 v_G^2}{\omega^2}\right) = k^2 D_G^2 + \frac{4\pi i\omega}{c^2}\frac{k_1^2}{8\pi}\frac{1}{\varepsilon_{G1}}\left(\chi_{G1}\phi_{gp_1} + \chi_{Gb_1}\phi_{gp_{b1}}\right)\frac{k^2}{k_1^2}\left(\chi_{G1}\vec{v}_{G0} + \chi_{G1b}\vec{v}_{G0b}\right)$$

$$+ \frac{4\pi i\omega}{c^2}\frac{k_2^2}{8\pi}\frac{1}{\varepsilon_{G2}}\left(\chi_{G2}\phi_{gp2} + \chi_{Gb2}\phi_{gpb2}\right)\frac{k^2}{k_2^2}\left(\chi_{G2}\vec{v}_{G0}^* + \chi_{G2b}\vec{v}_{Gob}^*\right)$$

$$k^2 - \frac{\omega^2}{c^2} + \frac{\omega_{Gpp}^2}{c^2} + \frac{\omega_{Gpb}^2}{c^2}\left(1 + \frac{k^2 v_G^2}{\omega^2}\right) = k^2 D_G^2 + \frac{i\omega}{2c^2}\frac{k^2}{\varepsilon_{G1}}\left(\chi_{G1}\phi_{gp_1} + \chi_{Gb_1}\phi_{gp_{b1}}\right)\left(\chi_{G1}\vec{v}_{G0} + \chi_{G1b}\vec{v}_{G0b}\right)$$

$$+ \frac{i\omega}{2c^2}\frac{k^2}{\varepsilon_{G2}}\left(\chi_{G2}\phi_{gp2} + \chi_{Gb2}\phi_{gpb2}\right)\left(\chi_{G2}\vec{v}_{G0}^* + \chi_{G2b}\vec{v}_{Gob}^*\right)$$

$$k^2 - \frac{\omega^2}{c^2} + \frac{\omega_{Gpp}^2}{c^2} + \frac{\omega_{Gpb}^2}{c^2}\left(1 + \frac{k^2 v_G^2}{\omega^2}\right) = k^2 D_G^2$$

$$+ \frac{i\omega}{2c^2}\frac{k^2}{\varepsilon_{G1}}\left(\chi_{G1}{}^2\phi_{gp_1}\vec{v}_{G0} + \chi_{Gb_1}\phi_{gp_1}\chi_{G1}\vec{v}_{G0b} + \chi_{G1}\vec{v}_{G0}\chi_{Gb_1}\phi_{gp_{b1}} + \chi_{Gb_1}{}^2\phi_{gpb1}\vec{v}_{G0b}\right)$$

$$+ \frac{i\omega}{2c^2}\frac{k^2}{\varepsilon_{G2}}\left(\chi_{G2}{}^2\phi_{gp2}\vec{v}_{G0}^* + \chi_{Gb2}{}^2\phi_{gp2}\vec{v}_{Gob}^* + \chi_{G2}\chi_{Gb2}\phi_{gp2}\vec{v}_{G0}^* + \chi_{G2}\chi_{G2b}\phi_{gp2}\vec{v}_{Gob}^*\right)$$

substituting the value of $\phi_{gp1}, \phi_{gpb1}, \phi_{gp2}, \phi_{gpb2}$ as expressed in Equation of Annou and Tripathi[1], we obtain

$$k^2 - \frac{\omega^2}{c^2} + \frac{\omega_{Gpp}^2}{c^2} + \frac{\omega_{Gpb}^2}{c^2}\left(1 + \frac{k^2 v_G^2}{\omega^2}\right) = k^2 D_G^2$$

$$- \frac{i\omega}{4c^2}\frac{k^2}{\varepsilon_{G1}i\omega}\left(\chi_{G1}{}^2\vec{v}_{G0}\vec{v}_{G0}^* \cdot E + \chi_{Gb_1}\chi_{G1}\vec{v}_{G0b}\vec{v}_{G0}^* \cdot E + \chi_{G1}\vec{v}_{G0}\chi_{Gb_1}\vec{v}_{Gob}^* \cdot E + \chi_{Gb_1}{}^2\vec{v}_{G0b}\vec{v}_{Gob}^* \cdot E\right)$$

$$- \frac{i\omega}{4c^2}\frac{k^2}{\varepsilon_{G2}i\omega}\left(\chi_{G2}{}^2\vec{v}_{G0}^*\vec{v}_{G0} \cdot E + \chi_{Gb2}{}^2\vec{v}_{Gob}^*\vec{v}_{G0} \cdot E + \chi_{G2}\chi_{Gb2}\vec{v}_{G0}^*\vec{v}_{G0b} \cdot E + \chi_{G2}\chi_{G2b}{}^2\vec{v}_{Gob}^*\vec{v}_{G0b} \cdot E\right)$$

$$k^2 - \frac{\omega^2}{c^2} + \frac{\omega_{Gpp}^2}{c^2} + \frac{\omega_{Gpb}^2}{c^2}\left(1 + \frac{k^2 v_G^2}{\omega^2}\right) = k^2 D_G^2 - \frac{|v_{Go}|^2}{4c^2}\frac{k^2}{\varepsilon_{G1}}\left(\chi_{G1}^2 + \chi_{Gb_1}\chi_{G1}\frac{\vec{v}_{G0b}}{\vec{v}_{G0}} + \chi_{G1}\chi_{Gb_1}\frac{\vec{v}_{Gob}^*}{\vec{v}_{G0}^*} + \chi_{Gb_1}^2\left|\frac{\vec{v}_{G0b}}{\vec{v}_{G0}}\right|^2\right)$$

$$-\frac{|v_{Go}|^2}{4c^2}\frac{k^2}{\varepsilon_{G2}}\left(\chi_{G2}^2 + \chi_{Gb2}^2\left|\frac{\vec{v}_{G0b}}{\vec{v}_{G0}}\right|^2 + \chi_{G2}\chi_{Gb2}\frac{\vec{v}_{G0b}}{\vec{v}_{G0}} + \chi_{G2}\chi_{G2b}\frac{\vec{v}_{Gob}^*}{\vec{v}_{G0}^*}\right) \qquad (5)$$

substituting the value of perturbed plasma and beam velocities v_{Go} and v_{Gob} [1], one obtain

$$\vec{v}_{Go} = \frac{\phi_{go}k_o e}{m\omega_{Go}}$$

and $\vec{v}_{Gob} = \dfrac{\phi_{go}k_o e}{m(\omega_{Go} - k_o v_G)}\hat{z}$

$$k^2 - \frac{\omega^2}{c^2} + \frac{\omega_{Gpp}^2}{c^2} + \frac{\omega_{Gpb}^2}{c^2}\left(1 + \frac{k^2 v_G^2}{\omega^2}\right) = k^2 D_G^2 - \frac{|v_{Go}|^2}{4c^2}\frac{k^2}{\varepsilon_{G1}}\left(\chi_{G1}^2 + 2\chi_{Gb_1}\chi_{G1}\frac{\left(\frac{\phi_{go}k_o e}{m(\omega_{Go} - k_o v_G)}\right)}{\left(\frac{\phi_{go}k_o e}{m\omega_{Go}}\right)} + \frac{\chi_{Gb_1}^2}{\left(1 - \frac{k_o v_G}{\omega_{Go}}\right)^2}\right)$$

$$-\frac{|v_{Go}|^2}{4c^2}\frac{k^2}{\varepsilon_{G2}}\left(\chi_{G2}^2 + \frac{\chi_{Gb2}^2}{\left(1 - \frac{k_o v_G}{\omega_{Go}}\right)^2} + 2\chi_{G2}\chi_{Gb2}\frac{\left(\frac{\phi_{go}k_o e}{m(\omega_{Go} - k_o v_G)}\right)}{\left(\frac{\phi_{go}k_o e}{m\omega_{Go}}\right)}\right)$$

$$k^2 - \frac{\omega^2}{c^2} + \frac{\omega_{Gpp}^2}{c^2} + \frac{\omega_{Gpb}^2}{c^2}\left(1 + \frac{k^2 v_G^2}{\omega^2}\right) = k^2 D_G^2 - \frac{|v_{Go}|^2}{4c^2}\frac{k^2}{\varepsilon_{G1}}\left(\chi_{G1} + \frac{\chi_{Gb_1}}{\left(1 - \frac{k_o v_G}{\omega_{Go}}\right)}\right)^2$$

$$-\frac{|v_{Go}|^2}{4c^2}\frac{k^2}{\varepsilon_{G2}}\left(\chi_{G2} + \frac{\chi_{Gb2}}{\left(1 - \frac{k_o v_G}{\omega_{Go}}\right)}\right)^2$$

$$k^2 - \frac{\omega^2}{c^2} + \frac{\omega_{Gpp}^2}{c^2} + \frac{\omega_{Gpb}^2}{c^2}\left(1 + \frac{k^2 v_G^2}{\omega^2}\right) = k^2 D_G^2 - \frac{|v_{Go}|^2 k^2}{4c^2}\psi_G(\omega) \tag{6}$$

where

$$\psi_G(\omega) = \frac{1}{\varepsilon_{G1}}\left(\chi_{G1} + \frac{\chi_{Gb_1}}{\left(1 - \dfrac{k_o v_G}{\omega_{Go}}\right)}\right)^2 + \frac{1}{\varepsilon_{G2}}\left(\chi_{G2} + \frac{\chi_{Gb2}}{\left(1 - \dfrac{k_o v_G}{\omega_{Go}}\right)}\right)^2$$

$$k^2 + \frac{\omega_{Gpp}^2}{c^2} + \frac{\omega_{Gpb}^2}{c^2}\left(1 + \frac{k^2 v_G^2}{\omega^2}\right) = \frac{|v_{Go}|^2}{4c^2}\omega_{Go}\Theta\frac{k^2}{\omega^2 - \Theta^2} + k^2 D_G^2 \tag{7}$$

where another parameter

$$\Theta = \omega_{Go} - \left(\omega_{Gpp}^2 + k_1^2 v_{Gth}^2\right)^{1/2}$$

For the large value of k, we obtain

$$K^2 + \frac{\omega_{Gpb}^2}{c^2}\frac{K^2 v_G^2}{\omega^2} = \frac{|v_{Go}|^2}{4c^2}\frac{\omega_{Go}\Theta K^2}{\omega^2 - \Theta^2} + K^2 D_G^2$$

$$1 + \frac{\omega_{Gpb}^2}{c^2}\frac{v_G^2}{\omega^2} = \frac{|v_{Go}|^2}{4c^2}\frac{\omega_{Go}\Theta}{\omega^2 - \Theta^2} + D_G^2$$

$$\left(\omega^2 - \Theta^2\right)\left(\omega^2 + \frac{\omega_{Gpb}^2}{c^2}\, v_G{}^2\right) = \frac{|v_{Go}|^2}{4c^2}\, \omega_{Go}\Theta\omega^2 + D_G{}^2\omega^2\left(\omega^2 - \Theta^2\right)$$

$$\omega^4 + \omega^2\left(\frac{\omega_{Gpb}^2}{c^2}\, v_G{}^2\right) - \omega^2\Theta^2 - \frac{\omega_{Gpb}^2}{c^2}\, v_G{}^2\Theta^2 = \frac{|v_{Go}|^2}{4c^2}\, \omega_{Go}\Theta\omega^2 + D_G{}^2\omega^4 - D_G{}^2\Theta^2\omega^2$$

$$\omega^4\left(1 - D_G{}^2\right) + \omega^2\left(-\Theta^2 + \frac{\omega_{Gpb}^2}{c^2}\, v_G{}^2 + D_G{}^2\Theta^2 - \frac{|v_{Go}|^2}{4c^2}\, \omega_{Go}\Theta\right) - \frac{\omega_{Gpb}^2}{c^2}\, v_G{}^2\Theta^2 = 0 \qquad (8)$$

Equation (8) is quadratic in ω^2, hence it will give two roots.

The roots are

$$\omega^2 = \frac{\left(\Theta^2 - \dfrac{\omega_{Gpb}^2}{c^2}\, v_G{}^2 - D_G{}^2\Theta^2 + \dfrac{|v_{Go}|^2}{4c^2}\, \omega_{Go}\Theta\right) \pm \left[\left(-\Theta^2 + \dfrac{\omega_{Gpb}^2}{c^2}\, v_G{}^2 + D_G{}^2\Theta^2 - \dfrac{|v_{Go}|^2}{4c^2}\, \omega_{Go}\Theta\right)^2 + 4\left(1 - D_G{}^2\right)\left(\dfrac{\omega_{Gpb}^2}{c^2}\, v_G{}^2\Theta^2\right)\right]^{1/2}}{2\left(1 - D_G{}^2\right)}$$

In the case where $|v_{Go}|^2 = 0$ i.e., no pump wave or $\Theta = 0$, the growth rate defined by the roots with minus inside and plus outside,

$$2\left(1 - D_G{}^2\right)\omega^2 = \frac{\left(-\dfrac{\omega_{Gpb}^2}{c^2}\, v_G{}^2\right) \pm \left(\left(-\dfrac{\omega_{Gpb}^2}{c^2}\, v_G{}^2\right)^2\right)^{1/2}}{1}$$

$$2\omega^2 = \frac{-2\left(\dfrac{\omega^2_{Gpb}}{c^2}\,v_G{}^2\right)^2}{\left(1 - D_G{}^2\right)}$$

putting $\omega = \omega_r + i\gamma$ $\quad (|\gamma| \ll \omega_r)$

$$\gamma^2 = \frac{\omega^2_{Gpb}\,v_G{}^2}{c^2\left(1 - D_G{}^2\right)}\ ,$$

The growth rate of the unstable mode,

$$\gamma = \frac{\omega_{Gpb}v_G}{c\left(1 - D_G{}^2\right)^{1/2}} \tag{9}$$

where D_G is expressed as

$$D_G^2 = \frac{\beta_G}{i(\omega + i\eta_G)\varepsilon_{G1}}\chi_{G1}\left(\chi_{G1}\phi_{Gp_1} + \chi_{Gb_1}\phi_{Gp_{b1}}\right)\vec{E}$$

In the absence of the dust grains, equation (9) gives the similar expression of Annou and Tripathi [1].

CHAPTER 4

Results and Discussions

In this chapter we do the calculations using MATLAB software and typical dusty parameters for the study of the effect of dust grains on the growth rate of unstable mode.

The growth rate expression in presence of dust grains

$$\gamma = \frac{\omega_{Gpb} v_G}{c\left(1 - D_G^2\right)^{1/2}}$$

where

$$\omega_{Gpb} = \left(\frac{4\pi n_{Gb}^o e^2}{m_e}\right)^{1/2}$$

$$D_G^2 = \frac{\beta_G}{i(\omega + i\eta_G)\varepsilon_{G1}} \chi_{G1}\left(\chi_{G1}\phi_{Gp_1} + \chi_{Gb_1}\phi_{Gp_{b1}}\right)\vec{E}$$

In the absence of dust grains i.e., $\delta\left(= n_{Gio}\big/ n_{Geo}\right) = 1$, i.e., $\beta_G = 0$ we will get $\gamma = \frac{\omega_{Gpb} v_G}{c}$

which is the same expression as given by Annou and Tripathi [1]

We choose the typical dusty plasma parameters: ion plasma density $n_{Gi0} = 10^{10} \text{cm}^{-3}$, electron plasma density $n_{Ge0} = 10^{10}–10^9 \text{cm}^{-3}$ ($\delta = 1–10$), mass of ion $m_i = 40 \times 1836\ m_e$, temperature of electron Te = 1 eV, temperature of ion Ti = 0.1 eV, such that Ti/Te = 0.1, beam velocity of electron $V_{Gb0} = 2.5 \times 10^{10}$ cm/s, beam density of electron $n_{Gb0} = 3.6 \times 10^8 \text{cm}^{-3}$ and dust grain size a = 10^{-4} cm.

In figure 4.1, it can been seen that the growth rate of the unstable mode increases with the relative density of the dust grains.
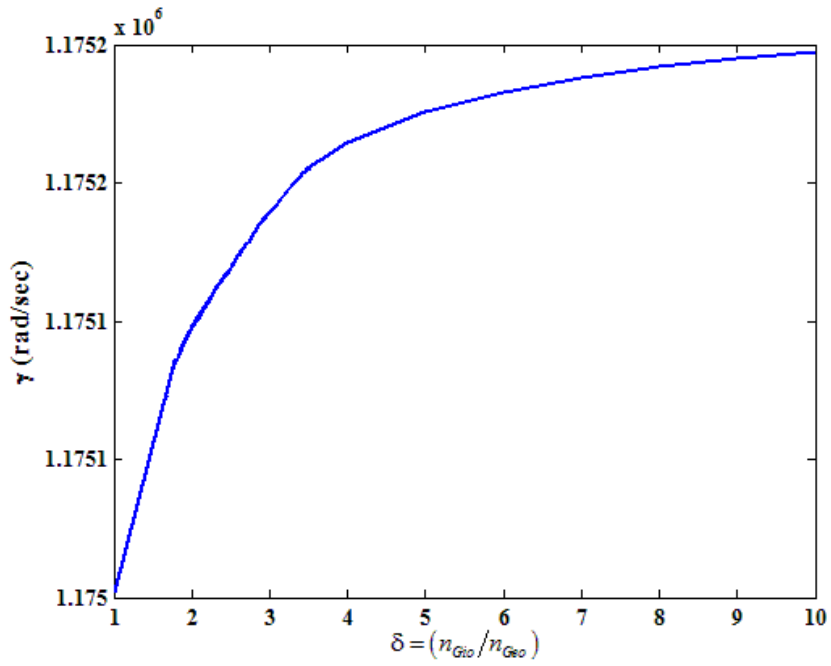
Figure 4.1 Variation of growth rate with δ (the relative density of dust grains)
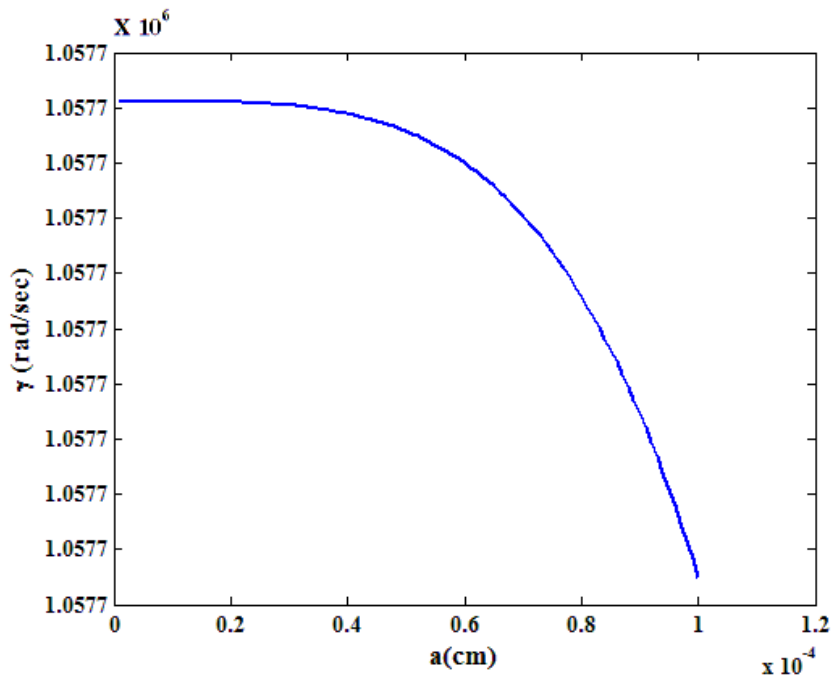
Figure 4.2 Variation of growth rate with dust grain size, a

From figure 4.2, we can say that the growth rate increases with reducing the dust grain size.
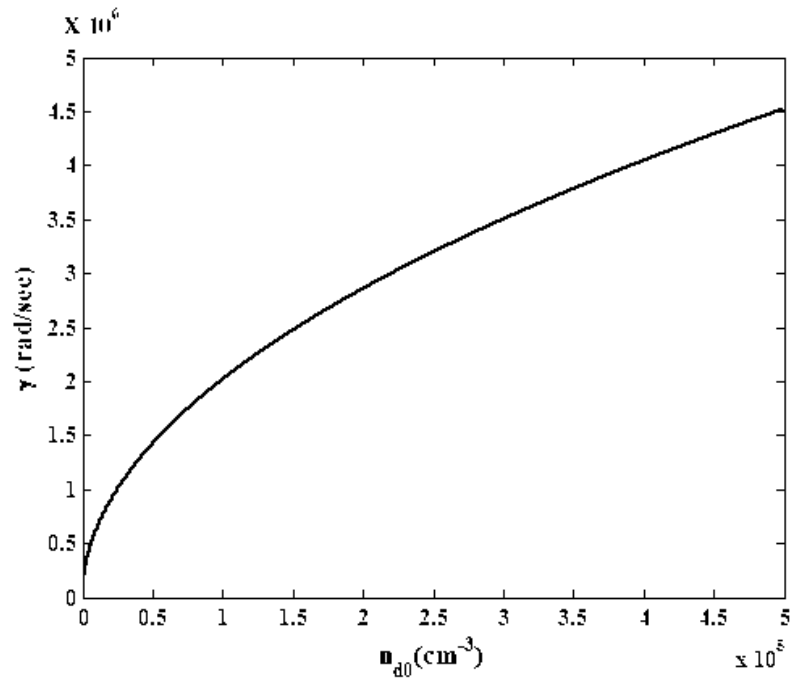
Figure 4.3 Variation of growth rate with dust grain density

From figure 4.3, it can be seen that the growth rate increases with dust grain density.

To summarize the result, in this dissertation we have studied and considered the effect of charged dust particles on the growth rate. It has been shown that the presence of charged dust grains modifies the dispersion properties of the wave.

REFERENCES

[1]ANNOU,R.,&TRIPATHI, V.K.,(1997). Phys. Letters A 226(1997) 193-195.

[2]UPADHYAY, A., AND TRIPATHI, V K.,(2002). Plasma Phys. Control. Fusion **44** (2002) 2357–2363

[3]VED PRAKASH, SURESH C. SHARMA, VIJAYSHRI, AND RUBY GUPTA(2012). Laser and Particle Beams, 2013

*[4] V.K. TRIPATHI AND C.S. LIU*, Phys. Fluids 25 (1982) 629.

[5] W.P. LEEMANS et al., Phys. Rev. A. 46 (1992) 1091.

[6]GUPTA, R., SHARMA, S.C. & PRAKASH, V. (2010). Phys. Plasmas 17, 1221051–1221056.

[7]SHARMA, S.C. & WALIA, R. (2008). Phys. Plasmas 15, 0937031–0937035.

[8]SHARMA, S.C. & SUGAWA, M. (1999). Phys. Plasmas 6, 444–448.

[9] LIU, C.S. & TRIPATHI, V. K. (2000). IEEE Trans. Plasma Sci. 28, 353–358.

[10]SHARMA, S.C. & SRIVASTAVA, M.P. (2001). Phys. Plasmas 8, 679–686.

[11]PRAKASH, V. & SHARMA, S.C. (2009). Phys. Plasmas 16, 0937031–0937039.

[12]PARASHAR, J., PANDEY, H.D. & TRIPATHI, V.K. (1998). J. Plasma Phys. 59, 97–102.

[13]SHARMA, R.P., MONIKA, A., SHARMA, P., CHAUHAN, P. & JI, A. (2010). Laser Parti. Beams 28, 531–537.

[14] SURESH C. SHARMA AND JYOTSNA SHARMA(2010).PHYSICS OF PLASMAS **17**, 043704 2010

[15]ANDERSON, M., GARATE, E., ROSTOKER, N., SONG, Y., VAN DRIE, A. & BYSTRITSKII, V. (2005). Laser and Particle Beams 23, 117–129.

[16]ANISIMOV, V.N., BARANOV, V.YU., DERKACH, O.N., DYKHNE, A.M., MALYUTA, D.D., PISMENNYI, V.D., RYSEV, B.P. & SEBRANT,A.YU. (1988). IEEE J. Quant. Electron. 24, 675–682.

[17]BIGONGIARI, A., RAYNAUD, M. & RICONDA, C. (2011). Phy. Rev. E 84, 0154021–0154024.

[18]BOUHELIER, A., IGNATOVICH, F., BRUYANT, A., HUANG, C., FRANCS, G. COLAS

DES, WEEBER, J.C., DEREUX, A., WIEDERRECHT, G.P. & NOVOTNY, L. (2007). Opt. Lett. 32, 2535–2537.

[19]BOYD, G.D., GOULD, R.W. & FIELD, L.M. (1961). Proceedings of the Institute of Radio Engineers 49, 1906–1916.

[20]CHEN, N.C., LIEN, W.C., LIU, C.R., HUANG, Y.L., LIU, Y.R., CHOU, C., CHANG, S.Y. & HO, C.W. (2011). Excitation of surface plasma wave at TiN/air interface in the Kretschmann geometry. J. Appl. Phy. 109, 0431041–0431047.

[21]EZAKI, M.A., KUMAGAI, H., TOYODA, K. & OBARA, M. (1995). IEEE J. Sel. Top. Quant. Electron. 1, 841–847.

[22]GHORBANALILU, M. (2012). Laser Part. Beams 30, 291–298.

[23]GIRKA, I.O., GIRKA, V.O. & PAVLENKO, I.V. (2011a). Progress in Electromagnetics Research 21, 267–278.

[24]GIRKA, V.O., GIRKA, I.O. & PAVLENKO, I.V. (2011b). Plasma Phys. Repts 37, 447–454.

[25]IRVINE, S.E., DECHANT, A. & ELEZZABI, A.Y. (2004) Phys. Rev. Lett. 93, 184801–184804.

[26]JANA, M.R., SEN, A. & KAW, P.K. (1993) Phys. Rev. E 48, 3930–3933.

[27]KRAFFT, C., THEVENET, P., MATTHIESSENT, G., LUNDIN, B., BELMONT, G., LEMBEGE, B., SOLOMON, J., LAVERGNAT, J. & LEHNER, T. (1994) Phys. Rev. Lett. 72, 649–652.

[28]LEE, M.J. & JUNG, Y.D. (2005). Z. Natursch. 60, 503–506.

[29]OSTRIKOV, K.N., YU, M.Y. & SUGAI, H. (1999). J. Appl. Phys. 86, 2425–2430.

[30]SHUKLA, P.K. & MAMUN, A.A. (2002). Introduction to Dusty Plasma Physics. Institute of Physics, Bristol, UK.

[31]SMOLYANINOV, I.I., ELLIOTT, J., ZAYATS, A.V. & DAVIS, C.C. (2005). Phy. Rev. Lett. 94, 0574011–0574014.

[32]https://en.wikipedia.org/wiki/Plasma_(physics)

Word Count: 3969

Plagiarism Percentage   8%

Matches

| 1 | **World Wide Web Match** |
| | View Link |

| 2 | **World Wide Web Match** |
| | View Link |

| 3 | **Database Match** |

| 4 | **World Wide Web Match** |
| | View Link |

| 5 | **World Wide Web Match** |
| | View Link |

| 6 | **Database Match** |

| 7 | **Database Match** |

| 8 | **Database Match** |

Suspected Content

ABSTRACT The primary objective of this work is development and validation of a code to check the role of dust grains on

the effect of a large amplitude Langmuir wave on the Weibel instabilities in plasma with an electron beam. The code checks the

2

growth rate of the destabilized wave with dust particles parameters as with that of dust density, dust grains size and ratio of ion and electron density. The electromagnetic perturbation pairs up with

the Langmuir wave to generate two Langmuir sideband waves which

2

is responsible for producing a current supporting and

enhancing the electromagnetic perturbation. The Langmuir wave enhances the growth over its linear value. The enhancement is larger at shorter wavelengths. **2**

CHAPTER 1 INTRODUCTION 1.1 General In plasma physics science,

waves in plasmas are interrelation of particles and fields which spreads and propagates in a periodically repeating fashion. Plasma is a quasi-neutral and electrically conductive fluid. In the most straightforward case, it is made up of electrons and **1**

positive ions but it may contain multiple ion including negative ions and neutral particles. A plasma couples to **1**

magnetic and electric field due to its electrical conductivity. A wide variety of wave phenomena is supported due to complex structure of particles and wave. Dusty plasma is a new frontier in modern technology and applied physics. Dusty plasmas are of our vast surroundings, for example,in the planetary ring system of Saturn, in Jupiter's moon. . Besides, there are additionally developing utilizations of charged dust in microbiology, in medicine, as well as in nanomedicine. In particular, an electro physical. 1.2 Historical Background the Orion Nebula , the noctilucent clouds, etc. A practically staggering number of images of astrophysical have flames because of particulates heated over 1000C. Thus, it is astonishing that the people of old considered flamess as a fourth state of matter, plasmas in our surrounding. and

magnetic and electric field due to its electrical conductivity. A wide variety of wave phenomena is supported due to complex structure of particles and wave. Dusty plasma is a new frontier in modern technology and applied physics. Dusty plasmas are of our vast surroundings, for example,in the planetary ring system of Saturn, in Jupiter's moon. . Besides, there are additionally developing utilizations of charged dust in microbiology, in medicine, as well as in nanomedicine. In particular, an electro physical. Figure 1 The current stresses the material used (by electric polarization) beyond its dielectric limit (in term a stage of electrical breakdown to an electric spark where the material transforms (as it becomes increasingly ionized, there is of a luminous similar to lightning) between the electrodes.

Plasma is a quasi-neutral and electrically conductive fluid. In the most straightforward case, it is made up of electrons and **1**

magnetic and electric field due to its electrical conductivity. A wide variety of wave phenomena is supported due to complex structure of particles and wave. Dusty plasma is a new frontier in modern technology and applied physics. Dusty plasmas are of our vast surroundings, for example,in the planetary ring system of Saturn, in Jupiter's moon. plasma which have an anisotropy (different value when measured in different directions) in momentum (velocity) space. This anisotropy is mostly understood as two temperatures in different directions. Burton Fried analysed that this instability can be understood easily as the superposition of number of counter-streaming beams. In this way, it is similar to the two- stream instability with the exception of that the perturbations are electromagnetic and leads in filamentation unlike to electrostatic perturbations which has an outcome in charge bunching. The instability causes exponential growth of electromagnet . . Table 1: Difference between Electron-ion plasma and Dusty plasma $nd0$ by $d=(3/4nd0)1/3$. The Debye in dusty plasma is given by $\frac{1}{D^2} = \frac{1}{Di^2} + \frac{1}{De^2}$ where $De = (Te / 4n e0 e^2)^{1/2}$ and it becomes important when $R << d < d$ $Z i$ $nio = neo + Z do$ ndo the grains emit electrons in UV irradiated dusty plasmas and they can be charged positively. Weibel instability is a plasma instability introduce in homogeneous or nearly homogeneous electromagnetic plasma which have an anisotropy (different value when measured in different directions) in momentum (velocity) space. This anisotropy is mostly understood as two temperatures in different directions. Burton Fried analysed that this instability can be understood easily as the superposition of number of counter-streaming beams. In this way, it is similar to the two-stream instability with the exception of that the perturbations are electromagnetic and leads in filamentation unlike to electrostatic perturbations which has an outcome in charge bunching. The instability causes exponential growth of electromagnetic fields in the plasma in the linear limit which will help in restoring momentum space isotropy. In rare cases, the Weibel instability is identified with one- or two- dimensional stream instabilities.

magnetic and electric field due to its electrical conductivity. A wide variety of wave phenomena is supported due to complex structure of particles and wave. Dusty plasma is a new frontier in modern technology and applied physics. Dusty plasmas are of our vast surroundings, for example,in the planetary ring system of Saturn, in Jupiter's moon. Chapter 3 Variation of Growth Rate Due to Dust 3.1 General Weibel instability is a plasma instability introduce in homogeneous or nearly homogeneous electromagnetic plasma which have an anisotropy (different value when measured in different directions) in momentum (velocity) space. This anisotropy is mostly understood as two temperatures in different directions. Burton Fried analysed that this instability can be understood easily as the superposition of number of counter-streaming beams. In this way, it is similar to the two-stream instability with the exception of that the perturbations are electromagnetic

and leads in filamentation unlike to electrostatic perturbations which has an outcome in charge bunching. The instability causes exponential growth of electromagnetic fields in the plasma in the linear limit which will help in restoring momentum space isotropy. In rare cases, the Weibel instability is identified with one- or two- dimensional stream instabilities. 3.2 Effect of Langmuir Wave on Weibel Instabilities

Plasma is a quasi-neutral and electrically conductive fluid. In the most straightforward case, it is made up of electrons and **1**

positive ions but it may contain multiple ion including negative ions and neutral particles. A plasma couples to **1**

magnetic and electric field due to its electrical conductivity. A wide variety of wave phenomena is supported due to complex structure of particles and wave. Dusty plasma is a new frontier in modern technology and applied physics. Dusty plasmas are of our vast surroundings, for example,in the planetary ring system of Saturn, in Jupiter's moon. plasma which have an anisotropy (different value when measured in different directions) in momentum (velocity) space. This anisotropy is mostly understood as two temperatures in different directions. Burton Fried analysed that this instability can be understood easily as the superposition of number of counter-streaming beams. In this way, it is similar to the two-stream instability with the exception of that the perturbations are electromagnetic and leads in filamentation unlike to electrostatic perturbations which has an outcome in charge bunching. The instability causes exponential growth of electro is recently experimentally conducted with the help of an anisotropic (different value when measured in different directions) electron velocity distribution function. = 0e-i(w t -k z) 00 (1) Where 0 = pp (1+ k02vth pp) 22 1/ 2 , pp=(4n0e2m), 0 1/ 2 m and e are the mass and electronic charge. - n0 b ek020 0 n0b = , m(0-k0vs) 2 -0 k0 e v0 b = ^ z m(0-k0vs) (2)

Now we can perturb the equilibrium by an electromagnetic perturbation c E=Ee-i(t -k.x),B= kÃ—E **3**

1=1e(-iwt-kr) 11 and 2=2e(-i w t -k r) 2 2 (3) Where 1,2 = Â± o and k1,2 = kx Â± k o z . ^ ^ ek11 v1b = - m(1 - k1z vs) nobek121 o n1b = - (4) m(1 - k1z vs)2 e1 k1 v1 = - and m1 k12 n1 = 11 , (5) 4e - (pp + k12 vth) 2 2 1 Where 12 is the plasma electron susceptibility. 1

1 1 1 J NL = - n1ev0 - n2 ev0 - n1b ev0 **8**

b - n2 b ev 0 b 2 2 2 2 k12 k2 =- (11v0 + 1b1v0b) - 2 (22v 0 + 2b2v0b) (6) 8 8 J L = - n0 ev - n0 b evb - nb evs 0 0 (7) eE kvs vb = z+ ^ ^ x; mi ek 2 vs nb = n 0 E (8) mi 0b Where we have considered E z J L can be written as ^, -e2 E 0 0 0 k vs 22 e2 kvs J= L n0 + n0b + n0b 2 z - n0b ^0 ^ Ex mi (9) mi e Fp1 = - vo Ã— B = iek p1 , 2c e Fp 2 = - vo Ã— B = iek p 2 , (10) 2c Where p= v0 E ; and 2i 1 1 p = - v0 E 2 2i k2 nNL = 1 p1 , 4e 1 k2 n NL = 2p2, 4e 2 k2 n1NL = b1 pb1 , 4e b k2 n NL = b 2 pb 2 , (11) 4e 2b Where 1 p= v0 b E ; 2i b1 1 p= v0 b E b2 2i Substituting the value of in the Poisson's equation, we can obtain 11=-(1p+ b p) k2 1 1 b1 k 12 22=-(2p+ b p) k2 2 (12) 2 2 b2 k2 Where pp + k1,2 vth 2 12 pb2 1,2 = 1- - 1,2 (1,2 - k1,2 z vs)

2 Using equation (6)), we have 4i (J)+ 2 Ã—Ã—E = L + J NL E c2 c2 We can write = ik ; k . E = 0 Substituting the above value in wave equation, one have -4i e2 E1 0 0 0 k vs ( ) 0 e kvs 22 2 k E1 - k kE1x = 2 2 ^ n0 + n0b + n0b 2 z + n0b ^ ^ E1x c mi mi k12 2 2 + (11v0 + 1b1v0b) + (22v0 + 2b2vob) + 2 E1 k2 8 8 c -4 i e2 E1 0 0 2 22 0 k vs k E1 - 2 E1 - n+n+n z 2 ^ c c2 mi 0 0b 0b 2 -4 i 0 e2 kvs ^ k12 E1 x + (11v0 + 1b1v0b) + 2 (22v0 + 2b2vob) + k (kE1x) k2 = n0b ^ c2 mi 8 8 4 e2 E1 m pp 4 e2 E1 m pb m pb k 2vs2 2 2 2 2 k E1 - 2 E1 + 2 + + = LHS (13) c mc2 4 e2 mc2 4 e2 4 e2 2 Where m pb 2 n0 = ; 4e2 0b m pp 2 n=0 4e2 0 Now on arranging and solving the equation (13), we have on LHS as 2 pp pb k 2vs2 22 k-2+2+21+2 =LHS 2 (14) ccc 3.3 Effect of Dust Grain on Weibel Instability To check the effect of dust grain, let us consider the wave equation and dust grain parameters such as dust susceptibility and dust densities. 4iL 2 - E+(E)E=2(J+J)+2E 2 NL (15) c c Substituting the value of E = -4 ndoQd 1 in above equation (15), we have -4 i e2 E1 0 0 0 k vs 22 e2 kvs k E1 + (-4 ndoQd1) E = 2 2 n0 + n0b + n0b 2 z ^ + n0b 0 E1x ^ c mi mi k12 2 2 + (11v0 + 1b1v0b) + (22v0 + 2b2vob) + 2 E1 k2 8 8 c Now considering dust term in RHS, we have -4i k12 2 RHS = 2 (11v0 + 1b1v0b) + (22v0 + 2b2vob) } - (-4 ndoQd1) E k2 c8 8 Substituting the value of I eo n e1 Qd1 = - i(+i) neo k12 pp k12vth 2 2 k12 And ne1 = 11 = - - 2 , we have 4 e 4 e 12 1 -4i k12 2 Ieo 1 k12 = 2 (1v0 + 1b1v0b) + (22v0 + 2b2vob) } + 4ndo k2 - 1E c8 8 i(+i) neo 4e 1 1 Let us consider I eo n do = e n eo -4i k12 2 k12 = 2 (1v0 + 1b1v0b) + (22v0 + 2b2vob) } + k2 -1 E c8 8 i(+ i) 1 1 1 Substituting the value of 1 and 2 , we have -4i k12 k12 k2 ( ) 2 = 2 1 (1v0 + 1bv0b) + 2 (2v0 + 2bvob) } + k2 i(+ i) 1 p1 + b1pb1 k2 E c8 8 1 1 1 - 4 i k12 k 22 = 1(1v0+ 1bv0b)+ 2(2v0+ 2bvob) }+k2Gp 2 8 8 2 c Where G p = 2 1(1p+ b p)E i(+i)1 1 1 b1 4 i k12 1 =kG+2 2 2 c8 1 p k2 1 p1 + b1 pb1 2 (1v0 + 1b v0 b) k1 ( ) 4ik221 k2 + (2p2+ b2pb2)2(2v0+ 2bvob) c8 2 2 k2 ik2 =kG+2 2 2c 1 2 p (1 p1 + b1 pb 1)(v1 0 + 1b v 0 b) ik2 +2 2c 2 (2p2+ b2pb2)(2v0+ 2bvob) ik2 =k G + 2 2c 1 2 1 2 p1 v 0 + b1 p1 1 v 0 b + 1 v 0 b1 pb 1 + b1 2 pb1 v 0 b 2 p ( ) ik2 + 2c 2 2 (22p2v0+ b22p2vob+ 2 b2p2v0+ 2 2bp2vob) Substituting the value of p1, pb1, p 2 , pb 2 as expressed in Equation (10) and Equation (11), we get ik2 =kG-2 2 4c 1i 12v0v0 E + b1 1v0bv0 E + 1v0 b1 vob E + b1 2v0bvob E 2 p ( ) ik2 -2 4c 2i (22v0v0 E + b22vobv0 E + 2 b2v0v0b E + 22b2vobv0b E) k2 2 v0b 2 2 vo v0b v ob =k2Gp- 2 1 + b1 1 + 1 b1 + b1 2 4c 1 2 v0 v0 v0 vo k 2 2

v 2 2 2 v0b v - 2 + b2 + 2 b20b+ 2   **7**

2bob 4c 2 2 v0 v0 v0 Substituting the value of vo and vob, o koe vo = mo okoe vob = ^ z m (o - ko vs) we have o koe m(o-kovs) b1 2 2 vo k 2 2 =k2Gp- 1 + 2 b1 1 + 2 2 4c 1 2 o koe kovs 1- mo o o koe m(o-kovs) 2 vo k 2 2 b22 - 2+ + 2 2 b2 4c 2 2 kovs 2 o koe 1- mo o 2 2 2 b1 2 2 vo k 2 - vo k + b2 =kGp-2 22 1+ 4c 1 4c 2

2 k o vs 2 k o vs 1-   **6**

1- o o 2 vo k 2 =k G - 22 p () 4c 2 Where 2 2 1 b1 + 1 + b2 ()= + 11 kv

2 2 kv 1- o s 1- o s o o   **5**

12 For ko 3o / c, mvs 1 kev and pp >> pb , we get for LHS=RHS 2 pp pb 2 k2vs2 vo 2 2 k2 k+ 2 + 1+2 = o 2 +k2Gp 2 c2 c2 4c 2 - 2 Where = o - (pp + k12 vth) 1 2 2 2 and kvth 0.3 pp . For the large value of k, 2 K 2vs 2 vo o K 2 2 K + pb 2 =22 +K2Gp2 c 22 4c - 2 pbvs2 2 2 v 1+ 2 =o22o2+Gp2 c 2 4c - 2 pb vs 2 vo o2 2 2 (-) + c2 = 4c2 2 2 + Gp22 (2 - 2) pb vs 2 2 2 pb vs 22 vo o2 2 2 2 +2 4 c 2 - - 2 = 2 + Gp24 - Gp222 c 4c

2pbv2 2 vo o 2 vs 22 2 4 (1- Gp2) + 2 - + 2 s + Gp22 - 2 - 2 pb =0 c 4c c The roots are 1 22v2 pb vs22 2 2 2v 2 v 2 v 2 2 -Gp22 + o 2 o ± - + pb s +Gp22 - o 2 o + 4(1-Gp2) 2 2 - s pb c 2 2 c 4c c 4c 2= 2(1-Gp2) considering vo = 0 or = 0 , the growth rate defined by the roots as 2 1 vs pb vs 2 2 22 2 - ± -2 c c 2 (1- Gp) = 22 1 pb 2 2 2 pbvs2 2 -2 2 c 22 = (1-Gp2) pb vs 2 2 =2 =r+i] c2(1-Gp2) , [as vs = pb c(1-G) 1 2 2 p vs Here = pb defines the growth rate. It might be noted that had been c(1-G) 1 2 2 p

positive we would have suppression of the Weibel instability.

3

CHAPTER 4 Results and Discussions This chapter present graph obtained from MATLAB code for the analysis and realization of the effect of dust grain on growth rate. In this thesis work we have obtain the value of growth rate in the presence of dust as vs = pb c(1-G) 1 2 2 p pb vs Without dust grains = = 1 , i.e., = 0 we will get nio neo = which is same as c the result given in research paper presented by R.Annou For performing the numerical calculations, we have used the typical parameters of the plasma wave: ion plasma density ni0 = 1015cm-31014cm-3 (= 1Â10), mass of ion mi = 40 Ã— 1836me ,temperature of electron Te = 1 eV, such that Ti/Te = 0.1 , electron plasma density ne0 = 1015,temperature of ion Ti = 0.1 eV, dust grain size a = 10-4 cm. , beam velocity vb0 = 2.5 Ã— 1010 cm/s, beam density nb0 = 3.6 Ã— 109cm-3 and In figure 1 and figure 2, it can been seen that the graph of growth rate increases almost linearly from a value 1.1751Ã—106 to 1.1752Ã—106 rad/ sec as changes from 1 to 2 and then increases slowly to maximum value at

=10. Figure 2 Figure 3 Figure 4 Figure 5 From figure

4

4, it can be easily analyzed as the size of the dust grain increases, the growth rate decreases and damped. Similarly from figure 5, it can be assured that as the dust density increases, there will be a marked variation of growth rate in decreasing order. To summarize the result, in this dissertation we have studied and considered the effect of charged dust particles on the growth rate. It has been shown that the presence of charged dust grains modifies the dispersion properties of the wave. CHAPTER 5 Scope for Future Studies In this dissertation, MATLAB code provides a basic knowledge in the area of the role of dust grains on

the effect of a large amplitude Langmuir wave on the Weibel instabilities in plasma with an electron beam.

2

This provides knowledge about the types of control algorithms which can be implemented in future, there advantages, disadvantages, etc. This dissertation provides knowledge about what will be those parameters which can be controlled to provide better performance of the system. There are various further areas where this dissertation will find the application. APPENDICES Appendix Parameters of Growth Rate MATLAB code has been used to express the graph between growth rate and dust grains parameters such as dust grain size, dust density and ratio of ion and electron density. A.1 MATLAB code for variation of growth rate with delta clc clear all; beta=82.78*10^4; phi1=2*10^24; k1=1.26; E=9; omega=151.91*10^18; omegap=356.74*10^9; vth=5.27*10^1; omega0=15.4*10^9; omega1=omega+omega0; c=3*10^10; m=9.1*10^-28; e=1.6*10^-19; ne=4*10^13; vs=sqrt(2000/(m)); ki1=-2; % ki1=-(((omegap^2)+ (k1*vth)^2)/omega1^2); omegab=sqrt(4*pi*0.04*ne*e^2/m); dt=1; endl=10; delta = 1:endl/dt; for i=1:endl/dt eta(i)=18*10^4/delta(i); gp(i)=((beta*eta(i)*k1^2*ki1*phi1*E)/(omega^2+eta(i)^2)); gama(i)=

```matlab
(omegab*vs)/(c*sqrt(1-gp(i))); % gama(i)=(omegab*vs)/(c); end figure,plot(delta,gama,'LineWidth',2);
xlabel('\delta'); ylabel('\gamma (rad/sec)');title('Variation of growth rate with delta');
```

A.2 MATLAB code for variation of growth rate with dust grain size

```matlab
clc clear all; phi1=2*10^24; k1=1.26; E=9;
omega=151.91*10^18; nod=5*10^4; omegap=356.74*10^9; vth=5.27*10^1; omega0=15.4*10^9;
omega1=omega+omega0; c=3*10^10; m=9.1*10^-28; e=1.6*10^-19; ne=4*10^13; vs=sqrt(2000/(m));
ki1=-2; % ki1=-(((omegap^2)+(k1*vth)^2)/omega1^2); omegab=sqrt(4*pi*0.04*ne*e^2/m); dt=1; dt1=10^-2;
endl=10^0; delta = 2; lemd=2; a=10^-3:dt1:endl; for i=1:endl/dt1 beta(i)=0.1*pi*a(i)^2*nod*vth; eta(i)=
((10^-2)*omegap*a(i))/(delta*lemd); % eta(i)=18*10^4/delta(i); gp(i)=
((beta(i)*eta(i)*k1^2*ki1*phi1*E)/(omega^2+eta(i)^2)); gama(i)=(omegab*vs)/(c*sqrt(1-gp(i))); % gama(i)=
(omegab*vs)/(c); end figure,plot(a,gama,'LineWidth',2); xlabel('a(cm)'); ylabel('\gamma
(rad/sec)');title('Variation of growth rate with dust grain size');
```

A.3 MATLAB code for variation of growth rate with dust density

```matlab
clc clear all; phi1=2*10^24; k1=1.26; E=9; omega=151.91*10^9; % nod=5*10^4;
omegap=356.74*10^9; vth=5.27*10^1; omega0=15.4*10^9; omega1=omega+omega0; c=3*10^10;
m=9.1*10^-28; e=1.6*10^-19; ne=4*10^13; vs=sqrt(2000/(m)); ki1=-2; % ki1=-(((omegap^2)+
(k1*vth)^2)/omega1^2); omegab=sqrt(4*pi*0.04*ne*e^2/m); delta = 2; lemd=2; a=10^-4; eta=
((10^-2)*omegap*a)/(delta*lemd); dt=10^1; endl=10^2; nod=1:dt:endl; for i=1:endl/dt
beta(i)=0.1*pi*a^2*nod(i)*vth; % eta(i)=18*10^4/delta(i); gp(i)=
((beta(i)*eta*k1^2*ki1*phi1*E)/(omega^2+eta^2)); gama(i)=(omegab*vs)/(c*sqrt(1-gp(i))); % gama(i)=
(omegab*vs)/(c); end figure,plot(nod,gama,'LineWidth',2); xlabel('n_{d0}(cm^{-3})'); ylabel('\gamma
(rad/sec)');title('Variation of growth rate with dust density');
```

1 2